

Photometric H α and [O II] Luminosity Function of SDF and SXDF Galaxies: Implications for Future Baryon Oscillation Surveys

Masanao SUMIYOSHI,¹ Tomonori TOTANI,¹ Shunsuke OSHIGE,¹ Karl GLAZEBROOK,² Masayuki AKIYAMA,³ Tomoki MOROKUMA,⁴ Kentaro MOTOHARA,⁵ Kazuhiro SHIMASAKU,^{6,7} Masao HAYASHI,⁶ Makiko YOSHIDA,⁶ Nobunari KASHIKAWA,⁴ and Tadayuki KODAMA⁴

¹Department of Astronomy, Graduate School of Science, Kyoto University, Kitashirakawa, Sakyo, Kyoto 606-8502
 sumiyosi@kusastro.kyoto-u.ac.jp

²Centre for Astrophysics and Supercomputing, Swinburne University of Technology,
 Mail H39, PO Box 218, Hawthorn, VIC 3122, Australia

³Astronomical Institute, Graduate School of Science, Tohoku University, Aramaki, Aoba, Sendai, Miyagi 980-8578

⁴National Astronomical Observatory of Japan, 2-21-1 Osawa, Mitaka, Tokyo 151-8588

⁵Institute of Astronomy, Graduate School of Science, University of Tokyo, 2-21-1 Osawa, Mitaka, Tokyo 181-0015

⁶Department of Astronomy, Graduate School of Science, University of Tokyo, Tokyo 113-0033

⁷Research Center for the Early Universe, School of Science, University of Tokyo, 7-3-1 Hongo, Bunkyo, Tokyo 113-0033

(Received 2000 December 31; accepted 2001 January 1)

Abstract

Efficient selection of emission line galaxies at $z \gtrsim 1$ by photometric information in wide field surveys is one of the keys for future spectroscopic surveys to constrain dark energy using the baryon acoustic oscillation (BAO) signature. Here we estimate the H α and [O II] line luminosity functions of galaxies at $z = 0.5$ –1.7 using a novel approach where multi-wavelength imaging data is used to jointly estimate both photometric redshifts and star-formation rates. These photometric estimates of line luminosities at high-redshift use the large data sets of the Subaru Deep Field and Subaru XMM-Newton Deep Field (covering $\sim 1 \text{ deg}^2$) and are calibrated with the spectroscopic data of the local Sloan Digital Sky Survey galaxies. The derived luminosity functions (especially H α) are in reasonable agreement with the past estimates based on spectroscopic or narrow-band-filter surveys. This dataset is useful for examining the photometric selection of target galaxies for BAO surveys because of the large cosmological volume covered and the large number of galaxies with detailed photometric information. We use the sample to derive the photometric and physical properties of emission line galaxies to assist planning for future spectroscopic BAO surveys. We also show some examples of photometric selection procedures which can efficiently select these emission line galaxies.

Key words: cosmology: observations – galaxies: statistics – techniques: photometric

1. Introduction

The precise measurements of the cosmological parameters in the past decade have shown that we live in a Universe whose expansion is accelerating (Riess et al. 1998; Perlmutter et al. 1999; Spergel et al. 2007; Komatsu et al. 2008). This has led to the paradigm of the Λ CDM universe whose acceleration is caused by a non-zero classical ‘cosmological constant’ (Λ), equivalent in effect to the energy density of the vacuum in relativistic quantum mechanics. Although this simple model is almost perfectly consistent with the cosmological data obtained so far, the value of Λ is unexplained and in fact 10^{121} times smaller than plausible physical values. These problems have motivate the generalisation of the accelerating component as a ‘dark energy’. The dark energy may be energy density of a still unknown physical field, or modification of the theory of gravity and spacetime on the cosmological scale may be required. To reveal the nature of dark energy has the potential to revolutionize our understanding of the universe and fundamental physics. (See, e.g., Copeland et al.

(2006) for a theoretical review.) A key question is whether the dark energy behaves exactly like Λ , or something more exotic. These cases can be distinguished observationally by higher precision measurements of the expansion history of the Universe.

One route to this expansion history is by using the baryon acoustic oscillation (BAO) method which has attracted particular attention in recent years as a promising new probe of dark energy (Blake & Glazebrook 2003; Seo & Eisenstein 2003; Glazebrook & Blake 2005). The BAO scale in the Universe serves as a ‘standard ruler’ whose length is determined by the sound horizon at the time of recombination and which imprints itself in the clustering of matter as revealed by the cosmic microwave background (CMB) at early times and the distribution of galaxies at later times. Because the BAO scale ($\simeq 150$ comoving Mpc) is set by straight-forward linear physics in the early Universe it is relatively robust against astrophysical uncertainties and can be calibrated by CMB observations (Eisenstein & White 2004). The BAO signatures have already been seen in the distribution of low-

redshift galaxies by the Two Degree Field Galaxy Redshift Survey (2dFGRS) (Cole et al. 2005) and Sloan Digital Sky Survey (SDSS) (Eisenstein et al. 2005; Tegmark et al. 2006; Percival et al. 2007; Okumura et al. 2008).

A clear next step is to detect BAO at higher redshifts, which would yield constraints complementary to those of low redshift surveys. A number of such BAO surveys are planned, including both spectroscopic and photometric surveys. In this paper we concentrate on spectroscopic BAO surveys at $z \sim 1$, which are optimal surveys because apparent BAO scales at $z \sim 1$ are the most sensitive to dark energy. However BAO surveys need to cover minimum volumes of order $1 h^{-3} \text{Gpc}^3$ in order to be effective (Blake & Glazebrook 2003) which implies survey areas of at least 500–1000 deg 2 . Since the largest fields of view on optical telescopes are of order 1 degree then for surveys to be feasible exposure times must be kept short (below one hour). Because of this star forming galaxies with emission lines are of particular interest, since we can determine the redshifts with a shorter exposure time. The emission lines useful for such surveys are likely to be the $[\text{O II}]\lambda 3727$ forbidden line doublet in optical spectroscopy, and $\text{H}\alpha \lambda 6563$ in near-infrared spectroscopy, both of which are well-known as representative star formation indicators (Kewley et al. 2004; Moustakas et al. 2006).

Important issues for such BAO surveys are (1) whether there are a sufficient number of emission line galaxies that can be detected with a reasonable exposure time, and (2) how to select them from photometric survey data as the targets of spectroscopic observations. These issues can be examined by analysing the existing estimates of the luminosity functions of emission line galaxies at $z \gtrsim 1$, based on slitless spectroscopic surveys (Yan et al. 1999; Hopkins et al. 2000 in $\text{H}\alpha$), photometry-selected spectroscopic surveys (Tresse et al. 2002 in $\text{H}\alpha$; Hogg et al. 1998; Teplitz et al. 2003; Zhu et al. 2008 in $[\text{O II}]$), photometric surveys using narrow-band filters (Geach et al. 2008 in $\text{H}\alpha$, Ly et al. 2007; Takahashi et al. 2007 in $[\text{O II}]$), and Fabry-Perot spectroscopic surveys (Hippelein et al. 2003 in $[\text{O II}]$). However, the statistics of these studies (especially $\text{H}\alpha$) are rather limited, because of the small survey area in spectroscopic surveys ($\lesssim 60 \text{ arcmin}^2$ for $\text{H}\alpha$) and small redshift range in narrow-band surveys ($\Delta z \sim 0.04$). In general BAO surveys are targeting bright and low number-density galaxies compared with those targeted in general studies of galaxy evolution, consequently limited statistics may lead to significant uncertainties due to small statistics and cosmic variances. Recently Zhu et al. (2008), covering a large area ($\sim 14,000$ galaxies in 2.45 deg $^{-2}$), has appeared but this is the only large $[\text{O II}]$ survey.

Here we study these issues based on wide-field broad-band photometric data of the Subaru Deep Field (SDF) (Kashikawa et al. 2004) and the Subaru XMM-Newton Deep Field (SXDF) (Furusawa et al. 2008), with estimating redshifts and emission line luminosities from star formation rate based on the photometric redshift calculations. Although the redshift and emission line luminosity estimates are less reliable than those of spectroscopic or

narrow-band surveys, the statistics is greatly improved by the SDF and SXDF data, which are the deepest data among the surveys covering $\gtrsim 1 \text{ deg}^2$. Furthermore, deep photometric data in a variety of band filters allow us to examine the photometric properties of emission line galaxies in detail, to infer the required depth for imaging surveys and efficient procedures to select targets for spectroscopic observations.

We will present our results as far as possible in a general way so that they are useful for any BAO survey planning. To complement this we also examine the cases of specific BAO survey proposals. Though there are several BAO surveys planned at $z \sim 1$, we examine the two proposed BAO surveys as examples. One is the FastSound project, which is a proposed BAO survey using the Fiber Multi-Object Spectrograph (FMOS), which is a new multi-fiber NIR spectrograph for the Subaru Telescope. FMOS has had engineering first light in May 2008 (Iwamuro et al. 2008) and is now undergoing further test observations. A BAO survey using $\text{H}\alpha$ emission line galaxies at $z \gtrsim 1$ has been proposed (Glazebrook et al. 2004a). The other is a BAO survey based on $[\text{O II}]$ emission line galaxies using the Wide-field Fiber-fed Multi Object Spectrograph (WFMOS) (Bassett et al. 2005), which is a proposed next-generation optical spectrograph for the Subaru Telescope having up to several thousand fibers.

This paper is organized as follows. In §2 we describe the photometric data sets used in this work and the methodology of photometric redshift calculations. In §3, we estimate the emission line luminosities with calibrations by the SDSS spectroscopic galaxy sample. We then calculate the $\text{H}\alpha$ and $[\text{O II}]$ luminosity functions and compare with those in previous studies, in §4. In §5 we discuss implications for future spectroscopic BAO surveys. Finally we show some examples of color selection of target galaxies for spectroscopic BAO galaxies in §6. We summarize our results in §7. Throughout this paper, we use the standard cosmological parameters of $H_0 = 70 \text{ km s}^{-1} \text{ Mpc}^{-1}$, $\Omega_m = 0.3$, $\Omega_\Lambda = 0.7$, $\Omega_b = 0.045$, $\sigma_8 = 0.8$ in the Λ CDM universe (Spergel et al. 2007). All magnitudes are given in the AB magnitude system.

2. The Sample and Photometric Redshifts

2.1. The SDF and SXDF Galaxies

The SDF is located at R.A. = $13^{\text{h}} 24^{\text{m}} 38^{\text{s}}.9$, Decl. = $+27^\circ 29' 25''$.9 (J2000), where the Galactic extinction is $E(B-V) = 0.017$ (Schlegel et al. 1998). All magnitudes presented below have been corrected for the Galactic extinction. We use the 0.114 deg^2 region where both the Subaru/Suprime-Cam data in $BVRi'z'$ bands (Kashikawa et al. 2004) and UKIRT/WFCAM data (Hayashi et al. 2007; Motohara et al. 2009, in preparation) in JK bands are available. The limiting magnitudes of the optical and NIR data are shown in Table 1. The seeing size of optical images is 0.98 arcsec FWHM (1 pixel = 0.2 arcsec). We use 19,494 galaxies detected both in i' and K bands. The requirement for K -band photometry is because of the need for accurate photometric redshifts and stellar contamina-

Table 1. Basic Information of SDF and SXDF

Field	Area [deg 2]	Number	Limiting magnitudes* [mag]								
			<i>B</i>	<i>V</i>	R_C	i'	z'	<i>J</i>	<i>K</i>	3.6 μ m	4.5 μ m
SDF	0.114	17408	28.5	27.7	27.8	27.4	26.6	24.0	24.3	—	—
SXDF	0.732	76193	28.1	27.8	27.6	27.6	26.6	24.5	24.0	23.1	22.4

* The limiting magnitudes are 3σ at 2'' aperture for B , V , R_C , i' , and z' bands, and 3σ at 3''.8 aperture for 3.6 and 4.5 μ m bands. For the J and K bands, they are 3σ at 2'' aperture (SDF) and 3σ at 2''.3 aperture (SXDF).

tion removal, however we will show below that this is not a significant source of bias.

The SXDF is centered at R.A. = 2^h 18^m 00^s.0 and Decl. = -5° 00' 00''.0 (J2000), where the Galactic extinction is $E(B - V) = 0.020$. We use the photometric data in $BVRi'z'$ bands (Furusawa et al. 2008) taken by Subaru/Suprime-Cam, in JK bands taken by UKIDSS survey (Warren et al. 2007), and in 3.6 and 4.5 μ m bands taken by SWIRE survey (Lonsdale et al. 2004), in the area of 0.732 deg 2 where the data in all of these bands are available. The details of the catalog will be reported elsewhere (Akiyama et al. 2009, in preparation). The limiting magnitudes are given in Table 1, and the seeing size of optical images is about 0.8 arcsec FWHM. As in the SDF we require K -band detection, and consequently we use 82,323 galaxies detected both in i' and K bands.

Stellar objects are removed as follows. For bright objects with $i' < 21.0$, we used the SExtractor (Bertin & Arnouts 1996) stellarity and objects are removed when the R -band CLASS STAR index is larger than 0.5. For objects fainter than $i' = 21.0$, we use the $Bz'K$ color-color diagram, and objects are removed if $(z' - K) < 0.5(B - z') - 0.8$ and $(z' - K) < 0.3(B - z') - 0.4$. (All galaxies selected by the detection in i' - and K -bands are detected also in B and z' bands.) After the removal of stars by these procedures, there remain 17,408 and 76,193 galaxies in the SDF and SXDF, respectively.

2.2. Photometric Redshift Estimate

We use the publicly available code *hyperz* (Bolzonella et al. 2000) for our photometric redshift estimations. We use 7 template models of spectral energy distribution (SED) having exponentially decaying star formation history with the characteristic time scales of $\tau = 0.1, 0.3, 0.7, 1, 3, 5$, and 15 Gyrs. In addition to this, we added a SED template with a constant star formation rate (SFR), and hence we have 8 SED templates in total. We use the stellar spectrum library of Bruzual & Charlot (2003) with the solar metallicity ($Z = Z_\odot = 0.02$) and the initial mass function of Salpeter (1955) in the mass range of 0.1–100 M_\odot . We apply the extinction law of Calzetti et al. (2000) for dust extinction ranging $A_V = 0.0$ –2.0 at an interval of 0.2. The stellar mass is estimated taking into account instantaneous recycling with a typical value of the returned mass fraction from evolved stars $R = 0.25$ (e.g., Nagashima & Yoshii 2004), as $M_* = (1 - R)M_{\text{SFR-int}}$, where $M_{\text{SFR-int}}$ is the stellar mass calculated by the integration of SFR through the star formation history of a galaxy. It is well known that the Salpeter IMF overestimates the number of low-mass stars compared to more realistic IMFs. We use

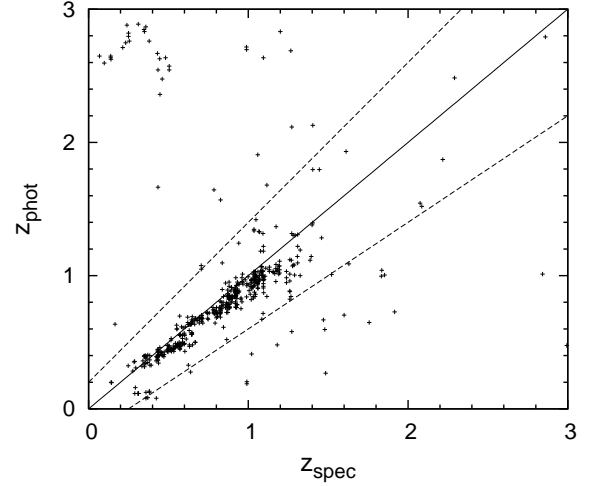


Fig. 1. Comparison of spectroscopic and photometric redshifts of SXDF galaxies. The solid and dashed lines show the lines of $z_{\text{phot}} = z_{\text{spec}}$ and $|z_{\text{phot}} - z_{\text{spec}}|/(1 + z_{\text{spec}}) = 0.2$, respectively.

the Salpeter IMF as it is convenient to use with *hyperz*, however we divide our final masses by 1.82 to convert them to the Baldry & Glazebrook IMF (Baldry & Glazebrook 2003) which is more realistic but has a particularly simple scaling with respect to the Salpeter IMF (Glazebrook et al. 2004b).

The photometric redshifts (z_{phot}) calculated in this way are compared with the spectroscopic redshifts (z_{spec}) of 550 X-ray undetected galaxies in SXDF having observed spectra (Figure 1). As in Ilbert et al. (2006), we define the redshift accuracy as the median of $1.48|\Delta z|/(1 + z)$, and outlier fraction as the fraction of those having $|\Delta z|/(1 + z) > 0.2$. The redshift accuracy and outlier fraction in $z_{\text{phot}} < 2.0$ and $z_{\text{spec}} < 2.0$ are 0.030 and 6%. This level of agreement is sufficient for the purposes of this work for most of the galaxies. It can be seen that galaxies at $z_{\text{spec}} \sim 0.3$ tend to be estimated as $z_{\text{phot}} \sim 3.0$, because of confusion between the 4000Å and Lyman breaks. However, since we are considering objects in the range $0.5 < z < 1.7$, this confusion will not affect our results. The photometric redshift distributions of SDF and SXDF galaxies in the different thresholds of K -magnitude are given in Figure 2.

In the following sections, we will mainly show the result of SXDF galaxies, because the photometric redshift calculations in SXDF are expected to be more reliable than those in SDF due to the advantage of having mid-infrared data.

3. Line Luminosity Calibration by SDSS Galaxies

We estimate emission line luminosities from SFRs of the best-fit SED templates in the photometric redshift calculations. Our primary goal is not to measure the SFRs themselves but rather use them as an intermediate step towards the final line luminosities. Accordingly rather than use standard conversion factors from line luminosity to SFR (e.g., Kennicutt 1998), we calculate our own conversion factors as part of our calibration process. This ensures we empirically obtain the best estimate of the relation between line luminosities and our photometrically estimated SFR, including systematic errors such as dust and metallicity effects. The calibration is done by using the large spectroscopic sample of local galaxies of the SDSS.

3.1. The SDSS Sample

We use the $u'g'r'i'z'$ photometric catalog publicly released from the SDSS studies at Max-Planck-Institute for Astrophysics / Johns Hopkins University¹, which is based on the fourth SDSS data release (Adelman-McCarthy et al. 2006). We select a sample with $14.5 < r_{\text{petro}} < 17.77$ and $0.023 < z < 0.399$ in order to detect $\text{H}\alpha$ and $[\text{O II}]$ lines in the wavelength coverage of SDSS, where r_{petro} is the Petrosian magnitude of r -band. We use the sample of star-forming galaxies constructed by Brinchmann et al. (2004), and the SDSS data set used in this work includes 75,757 objects, whose mean redshift is 0.081.

The SDSS photometric zero points are close to the AB convention but they are not reproduced exactly. We convert the SDSS photometry system into the AB system using the AB correction of Eisenstein et al. (2006). The SDSS spectroscopic observations cannot measure the total line emissions from galaxies, because of the limited size of the fiber diameter $3''$. We correct this aperture effect by the relation between Petrosian and fiber magnitudes as described in Hopkins et al. (2003).

3.2. Calibration

We use the *hyperz* on the SDSS $u'g'r'i'z'$ catalog for our photometric redshift estimations, as in the case of SDF and SXDF. In this work, we are interested in estimating observable line luminosities, rather than the true extinction-corrected line luminosity corresponding to SFR. Therefore we compare the SFR that is estimated by *hyperz* but reduced by the magnitudes corresponding to extinction ($A_{\text{H}\alpha}$ and $A_{[\text{O II}]}$), with the observed line luminosities ($L_{\text{H}\alpha, \text{obs}}$ and $L_{[\text{O II}], \text{obs}}$). The amount of extinction is calculated from the A_V estimates by *hyperz* and the adopted extinction law.

The correlation between the two quantities of the SDSS galaxies is shown in Fig. 3, for $\text{H}\alpha$ and $[\text{O II}]$ lines. It should be noted that we have corrected SFR estimates by an additional factor of $[d_L(z_{\text{spec}})/d_L(z_{\text{phot}})]^2$, to allow for the difference between the true spectroscopic redshift and

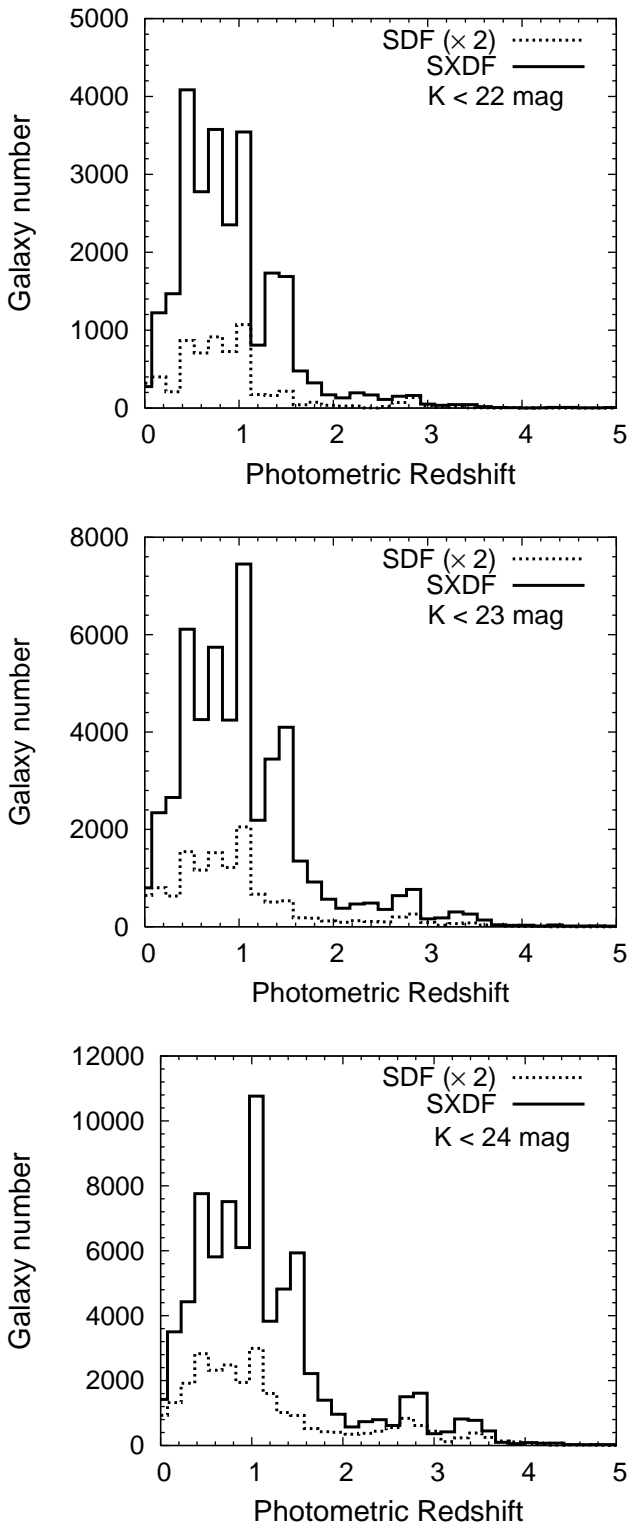


Fig. 2. The photometric redshift distributions of SDF and SXDF galaxies brighter than the K -magnitude of 22 (top), 23 (middle), and 24 mags (bottom). The number of SDF galaxies multiplied by 2 is shown in each panel.

¹ <http://www.mpa-garching.mpg.de/SDSS/>

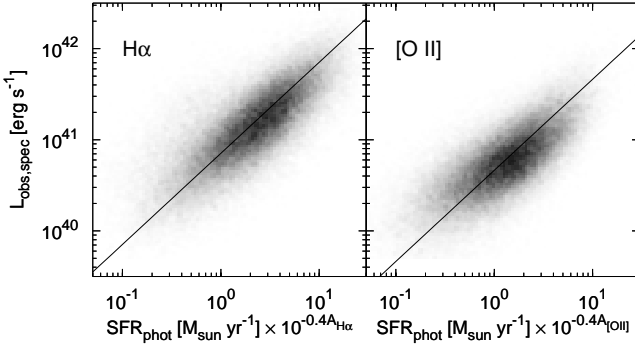


Fig. 3. The extinguished SFRs estimated by photometric redshift calculations versus H α and [O II] line luminosities measured by spectroscopic data of SDSS galaxies. The solid lines are the best-fit linear relation. The scatters in the case of H α and [O II] are ± 0.24 dex and ± 0.35 dex, respectively.

that returned by *hyperz*. For low-redshift samples such as SDSS a small redshift difference Δz does not significantly change the observed SED shape (as $\lambda\Delta z$ is much smaller than the band width) and hence the *hyperz* fit. However it has a much stronger effect on derived luminosities which is removed by this correction. We cross-checked this method of SFR estimates using a sub-sample of a few hundred SDSS galaxies where we manually adjusted *hyperz* to return the SED best fit at z_{spec} . We found the SFRs from the two approaches consistent to within a factor of two. We use the former approach as it is much more efficient for large samples with the existing *hyperz* codebase.

We see a tight correlation between SFR and H α luminosities, and we obtain the best-fit conversion relation as:

$$\log \left(\frac{L_{\text{H}\alpha,\text{obs}}}{[\text{erg s}^{-1}]} \right) = \log \left(\frac{\text{SFR}_{\text{phot}}}{[M_{\odot} \text{ yr}^{-1}]} \right) - 0.4A_{\text{H}\alpha} + 40.85.$$

The offset $+40.85$ is different from that of Kennicutt (1998) by 0.25 dex, which is not unreasonable considering the uncertainties in stellar spectrum libraries and efficiency of ionization photon production.

Next we consider the [O II] emission. As can be seen in the right panel of Fig. 3, the correlation with SFR is not as good as that of H α emission, which is almost certainly due to the effect of metallicity and extinction (Kewley et al. 2004; Moustakas et al. 2006). Hence, following Moustakas et al., we calibrate the conversion law from SFR to [O II] luminosities as a function of absolute *B*-band magnitude ($M_{B,\text{phot}}$) in order to remove the dominant luminosity dependence of these effects. Figure 4 shows the conversion factor, $\eta_{[\text{O II}]}$, versus absolute *B*-band magnitude, $M_{B,\text{phot}}$. Here the conversion factor is defined by the following equation:

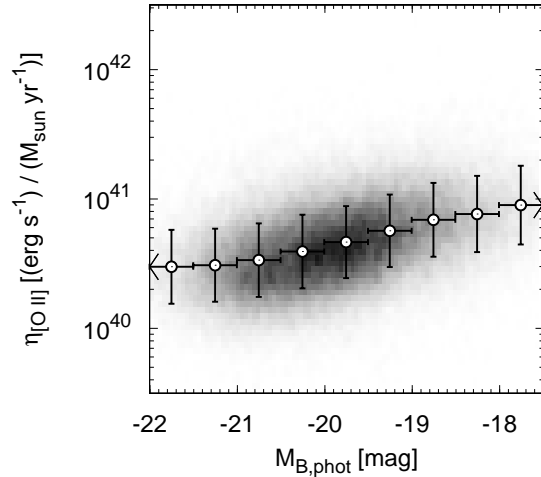


Fig. 4. The conversion factor $\eta_{[\text{O II}]}$ from SFR to [O II] line luminosity as a function of absolute *B*-band magnitude, $M_{B,\text{phot}}$. The small dots are the SDSS galaxies. The open circles and errors show the mean and standard deviation of the SDSS galaxy distribution in each $M_{B,\text{phot}}$ bin.

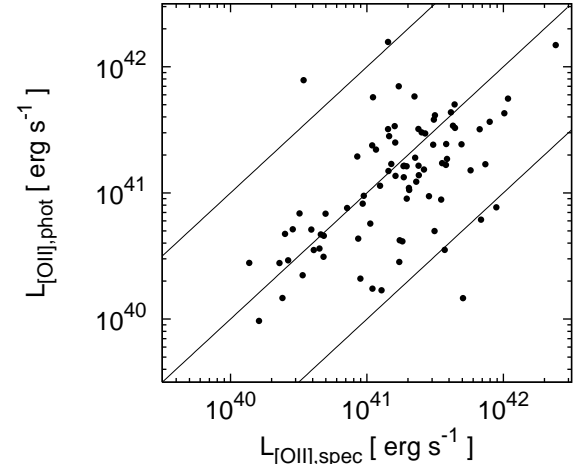


Fig. 5. Comparison of spectroscopic and photometric [O II] luminosities of SXDF galaxies with available spectra. The solid lines show the lines of $\log(L_{\text{O II}},\text{phot}/L_{\text{O II}},\text{spec}) = 0$ and ± 1.0 . The scatter is approximately ± 0.5 dex.

$$\log \left(\frac{L_{\text{[O II],obs}}}{[\text{erg s}^{-1}]} \right) = \log \left(\frac{\text{SFR}_{\text{phot}}}{[M_{\odot} \text{ yr}^{-1}]} \right) - 0.4A_{\text{[O II]}} + \log[\eta_{\text{[O II]}}(M_{B,\text{phot}})].$$

We derived $\eta_{\text{[O II]}}$ from calculating best fit values using SDSS data in every $M_{B,\text{phot}}$ bins, which are shown by open circles in Fig. 4. The best-fit formula of the conversion factor is given as follows:

$$\log[\eta_{\text{[O II]}}(M_{B,\text{phot}})] = 43.24 + 0.13M_{B,\text{phot}}.$$

One possible criticism of this calibration is that it is based on local galaxies and hence might not applicable to high- z galaxies (for example due to evolution in metallicity effects). We test this issue by using 88 SXDF galaxies with [O II] luminosities estimated from the emission line equivalent widths, and Figure 5 shows the comparison between photometric and spectroscopic [O II] luminosity estimates. Here we again correct the photometric line luminosity estimates by the factor of $[d_L(z_{\text{spec}})/d_L(z_{\text{phot}})]^2$ as for the SDSS sample, to remove the error coming from the distance estimate. The agreement between the two is reasonable though the scatter is significant ($\sim 0.5\text{dex}$). We also note also that Moustakas et al. showed that their approach for [O II] to SFR conversion worked reasonably well for galaxies at $z \simeq 1$.

4. Line Luminosity Functions

4.1. $H\alpha$ Luminosity Function

We construct the $H\alpha$ luminosity function per unit logarithmic luminosity interval in a given redshift interval (z_1, z_2), by simply dividing the observed number of galaxies by the comoving volume corresponding to the redshift interval. We do not use the more sophisticated $1/V_{\text{max}}$ method (e.g., Yan et al. 1999) to estimate LFs, because we cannot determine a clear limiting flux of $H\alpha$ emission for galaxies originally selected by broad band fluxes. Instead, we discuss the effect of limiting magnitudes on the LF estimates below.

The derived $H\alpha$ luminosity functions from SDF data (filled triangles) and SXDF data (filled circles) are shown in Figure 6, for three different redshift ranges of $0.5 < z < 1.0$ (top), $1.0 < z < 1.4$ (middle), and $1.4 < z < 1.7$ (bottom). We also plot the $H\alpha$ luminosity functions measured by previous studies, after correcting the cosmological parameter into those used in this work. The redshift ranges of the previous studies are slightly different from ours (see figure caption), and we plot the previous data in the panel of similar redshift ranges in this figure.

To examine the effect of limiting magnitudes on the LF results, the K -magnitude distributions of galaxies in several bins of $L_{H\alpha}$ are plotted in Figure 7. Since the K -band observation is relatively shallower than the i' band, we can examine the effect of the limiting magnitudes by comparing these distributions with the K -magnitude limits of SDF and SXDF. We find that the effect of limiting magnitude is not significant at $L_{H\alpha} \gtrsim 10^{41.4}, 10^{41.8}$, and $10^{42.0}$ erg/s for the redshift ranges of $z = 0.5-1.0$, $1.0-1.4$, and $1.4-1.7$, respectively, which are corresponding to

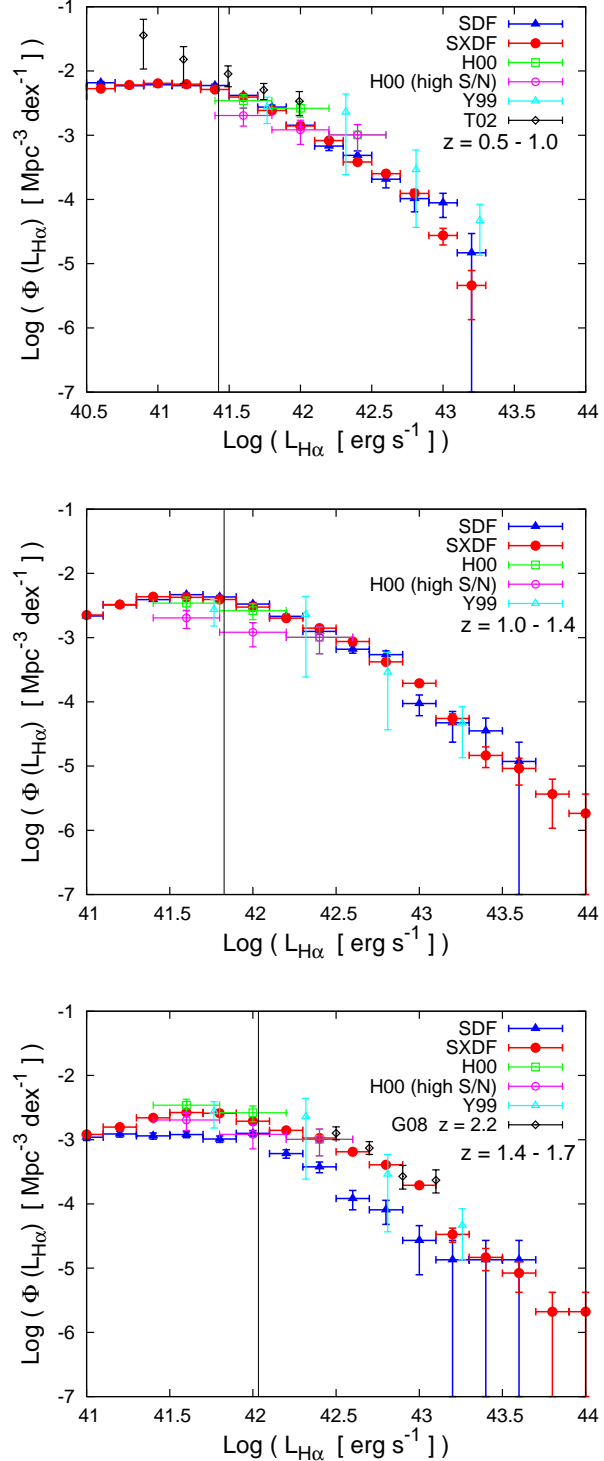


Fig. 6. The $H\alpha$ luminosity functions of SDF galaxies (filled triangles) and SXDF galaxies (filled circles) in $z = 0.5-1.0$ (top), $z = 1.0-1.4$ (middle), and $z = 1.4-1.7$ (bottom). The vertical lines indicate the luminosities corresponding to $F_{H\alpha} = 10^{-16} \text{ erg cm}^{-2} \text{ s}^{-1}$ at each redshift interval. Estimates by previous studies are also plotted, whose symbols are indicated in the figure. The redshift ranges of the previous estimates are as follows: Hopkins et al. (2000, H00) in $z = 0.7-1.8$, Yan et al. (1999, Y99) in $z = 0.7-1.9$, Tresse et al. (2002, T02) in $z = 0.5-1.1$, and Geach et al. (2008, G08) in $z \sim 2.23$, even though there is a small mismatch of redshift range. The “high S/N” data of Hopkins et al. (2000) are using only galaxies with spectroscopic confirmation or high S/N ratios. The data of G08 are obtained by a narrowband observation, while the others are spectroscopic observations.

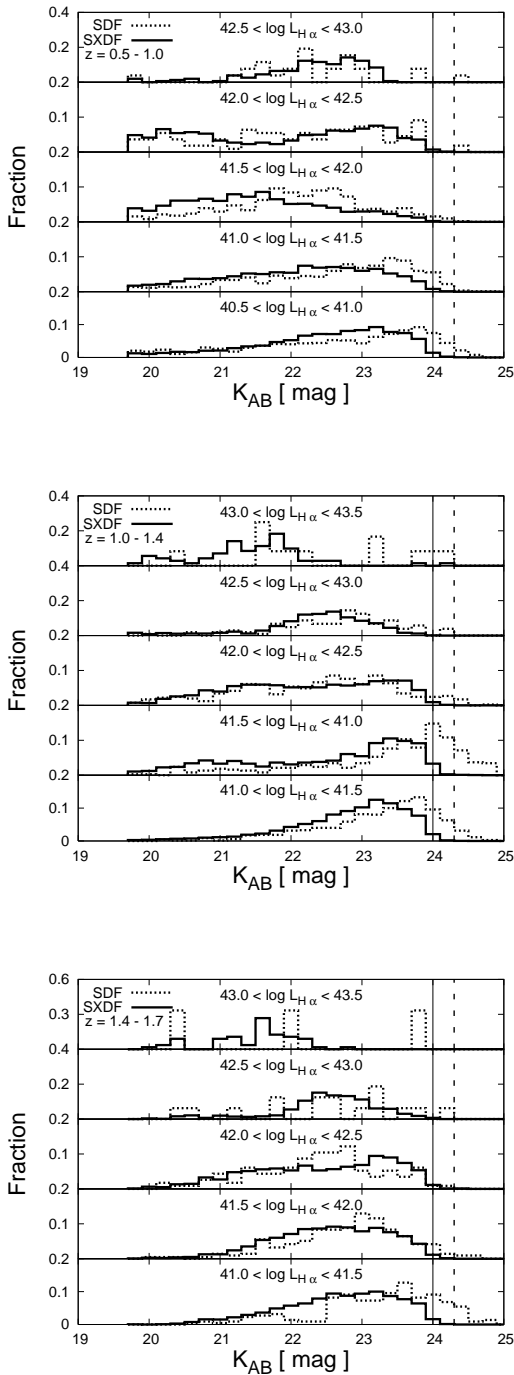


Fig. 7. The K -magnitude distributions of SDF (dotted) and SXDF galaxies (solid) in five $L_{H\alpha}$ (in erg/s) bins at $z = 0.5\text{--}1.0$ (top), $1.0\text{--}1.4$ (middle), and $1.4\text{--}1.7$ (bottom). The vertical lines are the K limiting magnitudes of SDF (dashed line, 3σ at $2''$ aperture) and SXDF (solid line, 3σ at $2''.3$ aperture).

the $H\alpha$ flux of $F_{H\alpha} \geq 10^{-16}\text{erg cm}^{-2}\text{s}^{-1}$. These luminosities are indicated by the vertical solid lines in Figure 6. Because galaxies for the BAO surveys considered in this work are brighter than this $H\alpha$ flux, the incompleteness does not seriously affect the main results of this work. As another test, we estimate the number of $H\alpha$ emission galaxies that are brighter than $F_{H\alpha} = 10^{-16}\text{erg cm}^{-2}\text{s}^{-1}$ but have been missed in our sample because of the requirement of K -band detection, by using the i' selected sample. In this case, we cannot use the $Bz'K$ diagram to remove stars and hence stellar contamination may increase, but we find that the number of bright emission galaxies increases at most 20% from our baseline analysis requiring K -band detection.

The agreement with the previous data derived by spectroscopic or narrow-band filter observations is reasonably good above the limiting magnitudes, providing some credence to our study based on photometric line luminosity estimates. However, the brighter-end of the LF at $z = 1.4\text{--}1.7$ estimated by the SDF data is significantly lower than those by the SXDF data and previous studies, which cannot be explained solely by the limiting magnitude effect. We find that the reason for this discrepancy is confusion between galaxies at $z \sim 0$ and $z \gtrsim 1.4$ due to the lack of the mid-infrared data in 3.6 and $4.5\text{ }\mu\text{m}$ bands in the SDF. We confirm this by checking that the LFs estimated by SXDF galaxies without using mid-infrared data are similar to those by SDF galaxies, thus the SXDF LF is preferred in the bottom panel of Figure 6.

4.2. [O II] Luminosity function

We also calculate the [O II] $\lambda 3727$ luminosity function in SDF and SXDF, which are shown in Fig. 8, as well as those by previous studies (see figure caption). The limiting magnitude effect is analyzed in the same way as with the $H\alpha$ luminosity function, by breaking it down in K -magnitude bins (Fig. 9). The figure shows that the limiting magnitude effect is not significant for $L_{[\text{O II}]} \gtrsim 10^{41.9}, 10^{41.3}$, and $10^{41.5}\text{ erg/s}$ at $z = 0.5\text{--}1.0, 1.0\text{--}1.4$, and $1.4\text{--}1.7$, respectively, which are corresponding to $F_{[\text{O II}]} \geq 10^{-16.5}\text{erg cm}^{-2}\text{s}^{-1}$. These luminosities are also shown by the vertical lines in Figure 8. As in the analysis of the $H\alpha$ LF, we estimate the number of [O II] emission galaxies brighter than $F_{[\text{O II}]} = 10^{-16.5}\text{erg cm}^{-2}\text{s}^{-1}$ using the sample selected by i -band detection regardless of the K -band detection, and we find that the increase of emission galaxies is at most $\sim 30\%$.

Although the results from different studies are reasonably consistent at $z = 0.5\text{--}1.0$ and $1.0\text{--}1.4$, the agreement is rather worse than for the $H\alpha$ LF. The reason could be due to the large scatter of the $L_{[\text{O II}]}-\text{SFR}$ relation or uncertainties in our calibration procedure. The paucity of galaxies at the faint end of our LF at $z = 1.0\text{--}1.4$ compared with previous studies is most likely due to the limiting magnitude effect. However, an even larger discrepancy is found at the faint-end of the LF at $z = 1.4\text{--}1.7$, which can not be explained solely by the limiting magnitude effect. (The disagreement between the [O II] LFs of SDF and SXDF is again caused by the lack of the mid-infrared

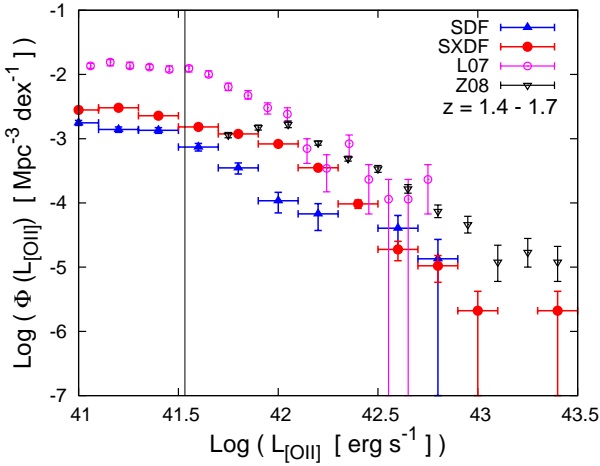
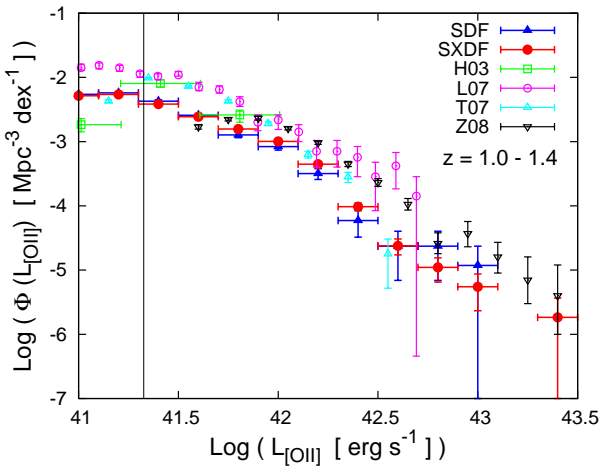
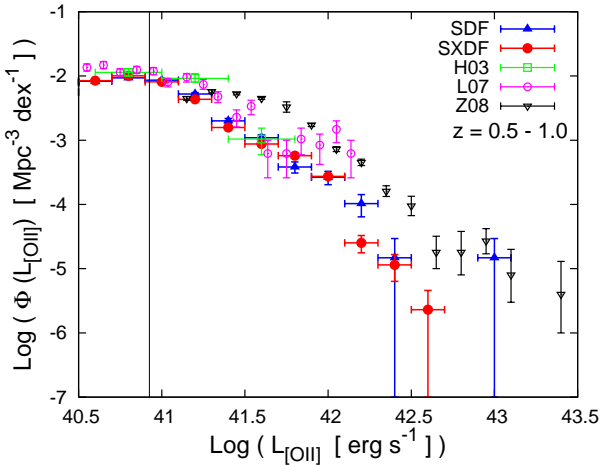


Fig. 8. The same as Fig. 6, but for [O II] line luminosity functions. The vertical lines indicate the luminosities corresponding to $F_{\text{O II}} \sim 10^{-16.5} \text{ erg cm}^{-2} \text{s}^{-1}$ on each redshift interval. The redshift ranges of the data of previous studies are as follows: Hippel et al. (2003, H03) at $z \sim 0.88$ (top panel) and ~ 1.18 (middle); Ly et al. (2007, L07) at $z \sim 0.89$ (top), $z \sim 1.19$ (middle), and $z \sim 1.47$ (bottom); Takahashi et al. (2007, T07) at $z \sim 1.19$ (middle); Zhu et al. (2008, Z08) at $z = 0.752-0.926$ (top), $z = 1.108-1.277$ (middle), and $z = 1.277-1.446$ (bottom). The data of H03 and Z08 are obtained by spectroscopic observations, while those of L07 and T07 are based on narrowband observations.

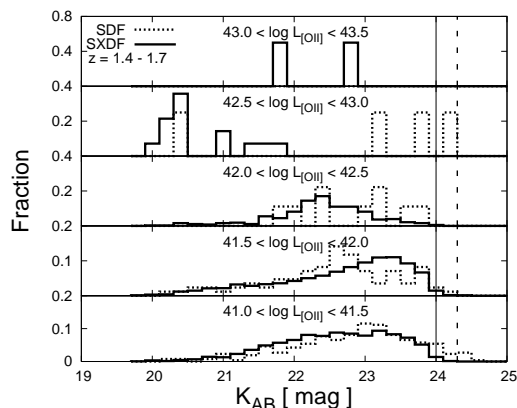
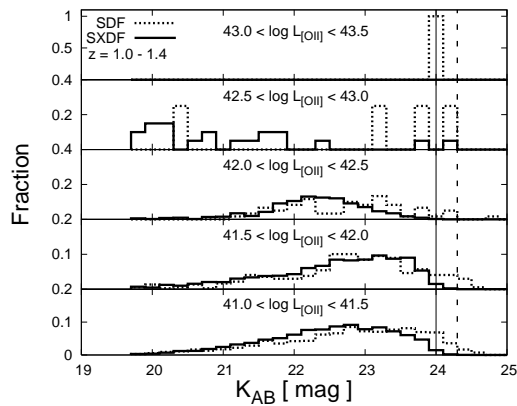
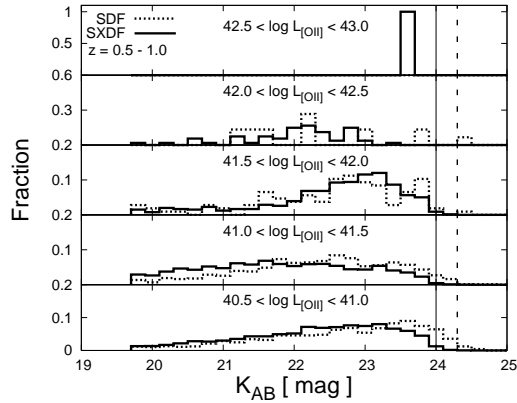


Fig. 9. The same as Fig. 7, but for [O II] line luminosity functions.

data in SDF.) One possibility is the contamination by different redshift emission line objects in the sample of Ly et al. (2007) which was selected by narrow-band photometry. However according to Ly et al. the contamination rate of their [O II] sample, estimated from their spectroscopic sample, is only 10–20%. The cosmic variance due to the small survey volume of Ly et al. may also have caused the discrepancy. Further systematic uncertainties in our photometric line luminosity estimates, such as the photometric redshift errors at $z > 1.4$ (see Fig. 1), may also be the origin of the discrepancy. Since the Ly et al. data is the only previous study that can be compared with the faint-end of our LF in this redshift range more data from independent studies are highly desirable.

5. Properties of Emission Line Galaxies

In this section we discuss implications for future BAO surveys, based on the emission line luminosity estimates obtained above. We intend to make our results as general as possible, but a specific discussion assuming existing proposals for future BAO surveys is also useful and illustrative. In particular, we discuss the proposed BAO surveys using FMOS and WFMOS as examples of H α and [O II] surveys, respectively. We consider three representative redshift ranges in the following analysis: $0.5 < z < 1.0$, $1.0 < z < 1.4$, and $1.4 < z < 1.7$, as used in the LF estimates. The whole redshift range $0.5 < z < 1.7$ roughly corresponds to the range that can be probed by optical [O II] and near-infrared H α surveys.

5.1. Galaxy Surface Density as Functions of Line Flux

First we check the available number of emission line galaxies in the three redshift intervals. These are the maximum numbers of emission line galaxies that can be used in any BAO survey. We plotted the cumulative number of SXDF galaxies as a function of H α and [O II] flux in Figure 10. The solid horizontal line in the panel indicates the surface number density of $nP = 1$ assuming $z \sim 1$, where n is galaxy number density and P is the amplitude of the power spectrum of galaxy density fluctuation at $k = 0.20 h \text{Mpc}^{-1}$, which is roughly the linear-nonlinear transition scale at $z \sim 1$. The survey power is maximized by choosing $nP = 1$ when the observing time is fixed (Seo & Eisenstein 2003; Glazebrook & Blake 2005). Here we used the formula of Eisenstein & Hu (1998) to calculate the CDM power spectrum. The linear clustering biases $b = 1.19$ and 1.17 are taken into account ($P_{\text{gal}} = b^2 P_{\text{CDM}}$) for H α and [O II] lines, respectively. These values are from the bias estimates for emission line galaxies at $1.0 < z < 1.4$ by stellar mass estimates, as described in §5.4.

We define $F_{\text{H}\alpha,\text{min}}$ as the flux above which the number of galaxies is equal to the surface number density corresponding to $nP = 1$, and hence $F_{\text{H}\alpha,\text{min}}$ gives the minimally required flux sensitivity to perform any BAO survey by emission line galaxies. We find that these values are $\log(F_{\text{H}\alpha,\text{min}}/[\text{erg cm}^{-2}\text{s}^{-1}]) = -15.5, -15.5$ and -15.8 for the redshift intervals of $0.5 < z < 1.0$, $1.0 < z < 1.4$ and $1.4 < z < 1.7$, respectively. These fluxes are brighter than

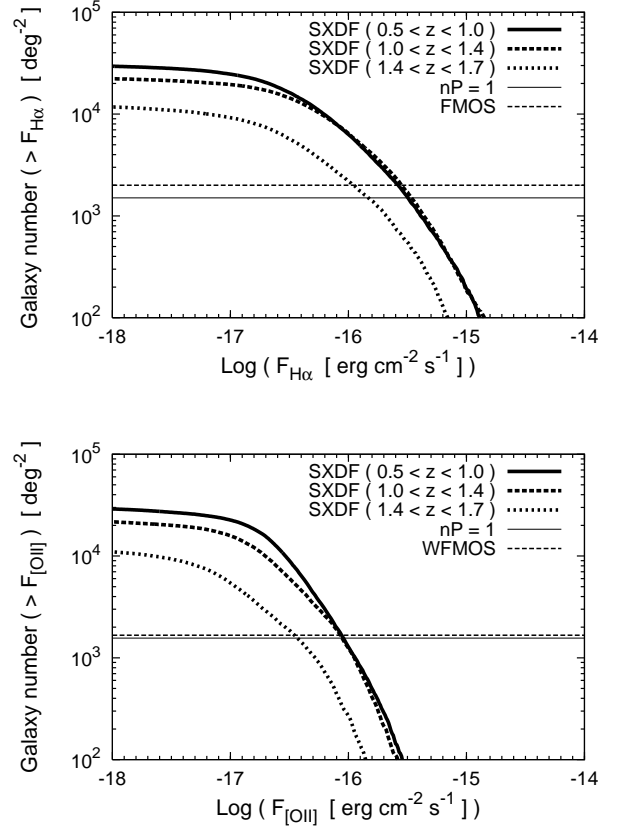


Fig. 10. The cumulative number counts of galaxies as functions of H α (top) and [O II] (bottom) flux. The solid, dashed, and dotted lines are for the redshift ranges of $0.5 < z < 1.0$, $1.0 < z < 1.4$, and $1.4 < z < 1.7$, respectively. The solid horizontal lines indicate the surface number density corresponding to $nP = 1$ at $z \sim 1$. (This density does not change significantly for the three redshift ranges.) The dashed horizontal lines represent the FMOS and WFMOS fiber density in the top and bottom panels, respectively.

the FMOS sensitivity, $\sim \log(F_{\text{H}\alpha}/[\text{erg cm}^{-2}\text{s}^{-1}]) = -16.0$ for 1 hour integration (Eto et al. 2004), and hence there are enough number of H α -emitting galaxies for a BAO survey by FMOS. The dotted horizontal line represents the fiber density of FMOS (400 in 0.2 deg^2), which is close to the galaxy number density corresponding to $nP = 1$, meaning that FMOS is an efficient instrument for a BAO survey than can collect a necessary number of galaxy spectra by one time observation per field, although BAO was not the original scientific target of this instrument.

Similarly, we define $F_{[\text{O II}],\text{min}}$ for [O II] line, and we find that these are $\log(F_{[\text{O II}],\text{min}}/[\text{erg cm}^{-2}\text{s}^{-1}]) = -16.1, -16.1$ and -16.4 for the three redshift intervals, respectively, which should be compared with the line sensitivity of WFMOS, $\log(F_{[\text{O II}]}/[\text{erg cm}^{-2}\text{s}^{-1}]) \sim -16.5$, for 0.5 hour integration (Parkinson et al. 2007). The horizontal dotted line is the planned fiber density of WFMOS (3000 in 1.8 deg^2). As in the case of H α line for FMOS, there is a sufficient number of emission line galaxies that can be used for a [O II] BAO survey by WFMOS.

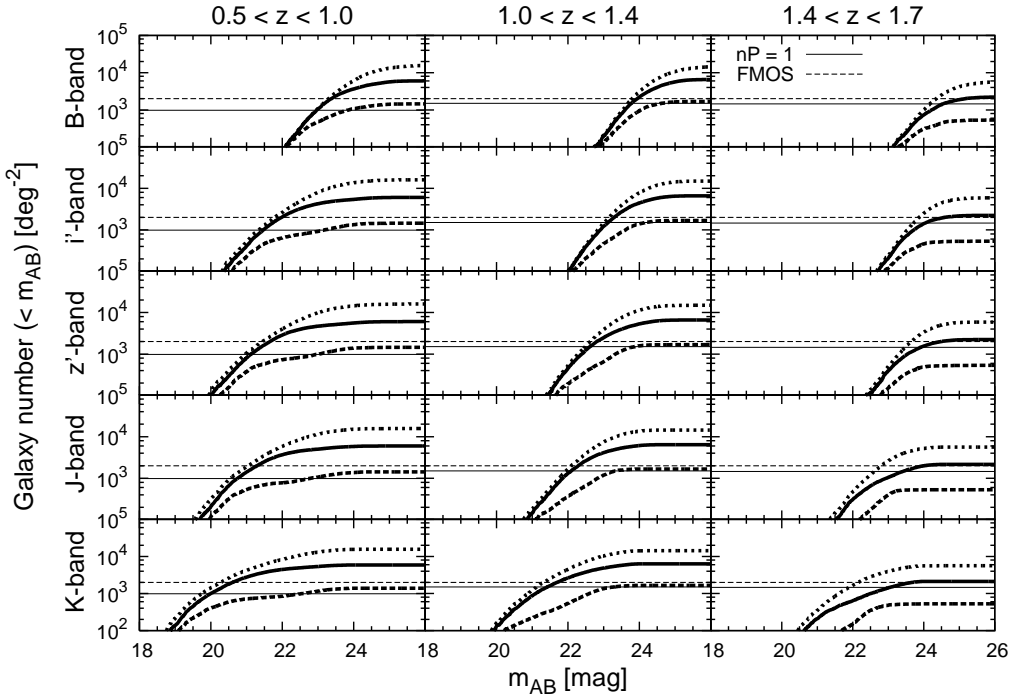


Fig. 11. The cumulative galaxy numbers of the H α emitting galaxies in SXDF as a function of magnitudes in popular band filters. They are shown separately for the three redshift intervals as indicated. The dashed, solid, and dotted lines show the number of emission line galaxies brighter than the three different threshold H α fluxes of $10^{-15.5}$, 10^{-16} , and $10^{-16.5}$ erg cm $^{-2}$ s $^{-1}$, respectively. The horizontal lines (solid and dashed) indicate the surface number density corresponding to $nP = 1$ at each redshift interval and the FMOS fiber density, respectively.

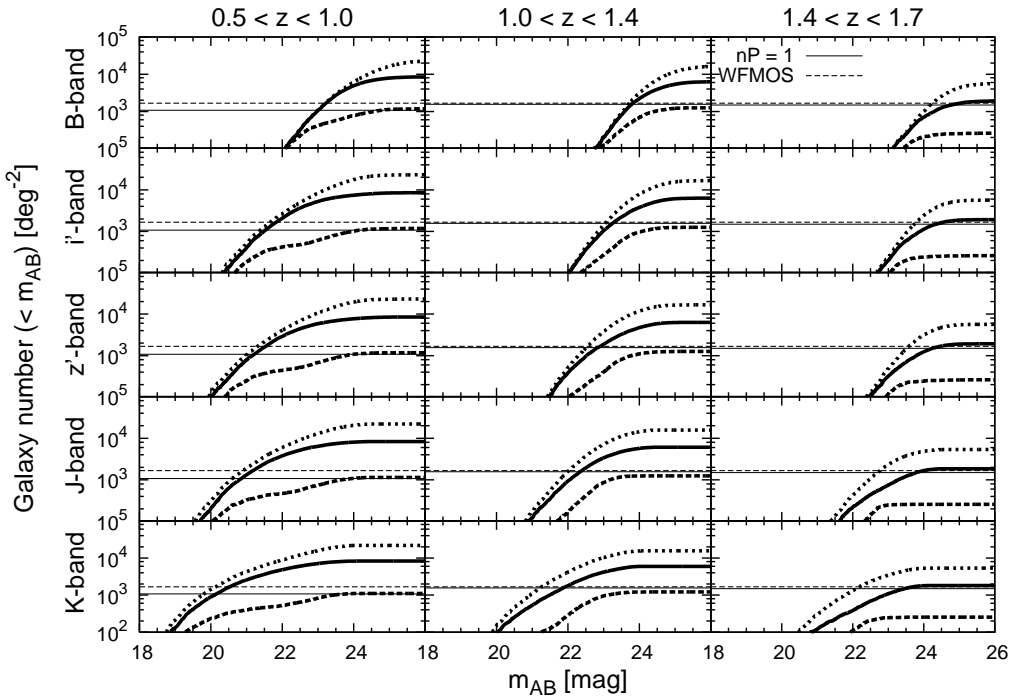


Fig. 12. The same as the Figure 11, but for the [O II] line. The dashed, solid and dotted lines are for the three different threshold [O II] fluxes of 10^{-16} , $10^{-16.5}$, and 10^{-17} erg cm $^{-2}$ s $^{-1}$, respectively. The horizontal lines (solid and dashed) indicate the surface number density corresponding to $nP = 1$ at each redshift interval and the WFMOS fiber density, respectively.

Finally we compare this result with that of the WiggleZ survey, a BAO survey targeting emission-line galaxies in the redshift range of $0.2 < z < 1.0$ (Glazebrook et al. 2007; Blake et al. 2009). The number of galaxies brighter than $F_{\text{[O II]}} = 10^{-16}\text{erg cm}^{-2}\text{s}^{-1}$ at $z=0.6-0.7$ by our estimates is 210 deg^{-2} , while that of actually observed by the WiggleZ survey is 35 deg^{-2} . The paucity of galaxy number of the WiggleZ is likely due to strong UV and r -band selection criteria of the survey.

5.2. Galaxy Surface Density as Functions of Broad-band Filter Magnitudes

Even if there are a sufficiently large number of galaxies for BAO surveys, they must be pre-selected by imaging surveys, and the required depth for such photometric selection is crucial in planning BAO surveys. Figure 11 shows the cumulative galaxy number of the H α emitting galaxies in SXDF as a function of magnitudes in popular band filters. They are shown separately for the three redshift intervals and different H α threshold fluxes as indicated. Figure 12 is the same as Figure 11, but for [O II] and WFMOS.

From these figures, one can infer the necessary (but not sufficient) depth in each band filter for photometric selection of targets. For example, we need imaging survey limits deeper than $B = 23.9$, $i' = 23.3$, $z' = 22.8$, $J = 22.3$, and $K = 21.7$ to detect BAO target galaxies brighter than the H α sensitivity of FMOS ($> 10^{-16.0} \text{ erg cm}^{-2}\text{s}^{-1}$) with a number density of FMOS fibers at $1.0 < z < 1.4$. Similarly, the required imaging depths for the WFMOS [O II] sensitivity ($> 10^{-16.5} \text{ erg cm}^{-2}\text{s}^{-1}$) become $B = 23.8$, $i' = 23.3$, $z' = 22.9$, $J = 22.4$, and $K = 21.9$. The similar magnitudes for FMOS and WFMOS indicate that the BAO targets for these two surveys have similar SFRs. While H α line luminosity is generally larger than [O II], NIR observations are less sensitive than optical observations, and hence the required integration time for Subaru becomes comparable for H α observed by FMOS and [O II] observed by WFMOS for a given SFR.

5.3. Stellar Mass, Extinction, and Size

Here we discuss some physical properties of the emission line galaxies that are useful for a planning of a BAO survey. First, we show the stellar mass distribution of SXDF galaxies that have been calculated in the photometric redshift estimates, in Figure 13 with the threshold fluxes of $10^{-16} \text{ erg cm}^{-2}\text{s}^{-1}$, for H α , or $10^{-16.5} \text{ erg cm}^{-2}\text{s}^{-1}$, for [O II] flux, in the three redshift intervals. We compare the mass distributions of these results with those of all galaxies in SXDF, and then we find that almost all galaxies which have small masses are emission line galaxies. The logarithmic means of the stellar mass distributions are presented in Table 2, for several different line flux thresholds. The mean stellar mass does not change significantly with the threshold line flux in a fixed redshift interval, and does not change either with redshift for a fixed threshold flux. The mean stellar mass of line emitting galaxies is rather low, but we note that there is quite a large spread of stellar masses from very massive galax-

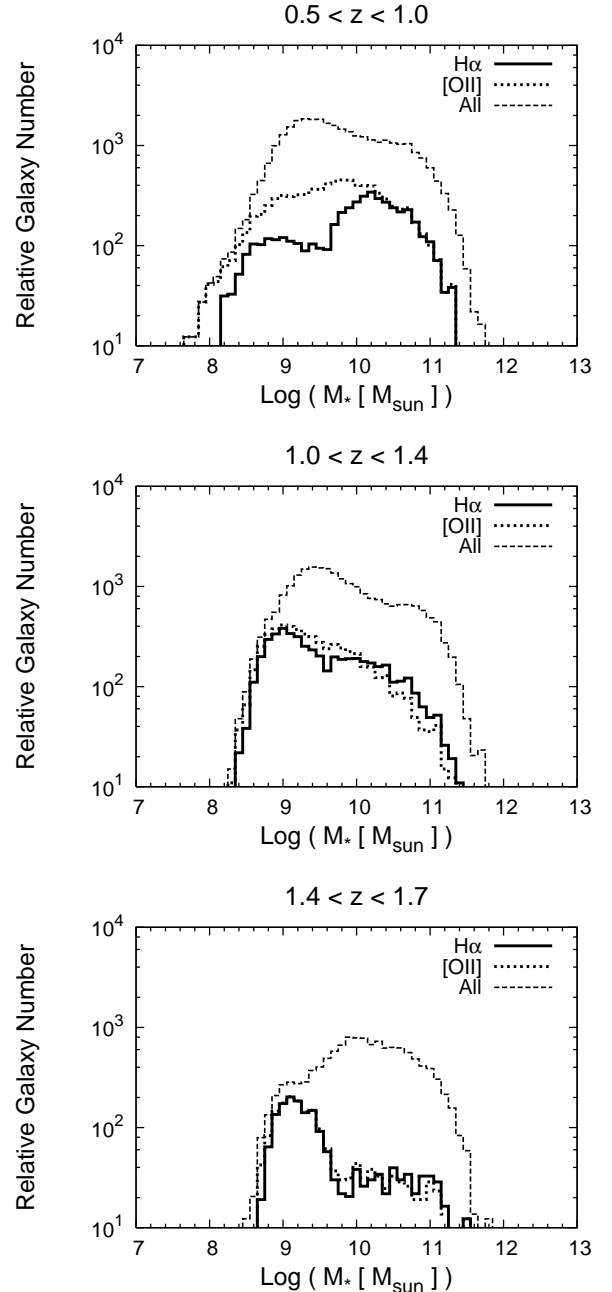


Fig. 13. The stellar mass distributions of H α and [O II] emission galaxies in SXDF at $z=0.5-1.0$ (top), $1.0-1.4$ (middle), and $1.4-1.7$ (bottom). The H α and [O II] threshold line fluxes are 10^{-16} and $10^{-16.5} \text{ erg cm}^{-2}\text{s}^{-1}$, respectively. We also show the mass distributions of all galaxies in the SXDF sample in the same redshift range, for the comparison with the results of emission line galaxies.

ies down to dwarfs. This result indicates that the line luminosity is not strongly correlated with stellar mass of galaxies.

Next we examine the extinction (A_V) distribution of SXDF galaxies estimated by the photometric redshift method in the three redshift ranges, as shown in Figure 14. The extinction is distributed with a large scatter, with

Table 2. Logarithmic means of the stellar mass of SXDF galaxies

Line flux [erg cm ⁻² s ⁻¹]	log M _* [M _⊙]*		
	0.5 < z < 1.0	1.0 < z < 1.4	1.4 < z < 1.7
log F _{H_α} > -16.5	9.8	9.7	9.9
log F _{H_α} > -16.0	9.9	9.6	9.6
log F _{H_α} > -15.5	9.7	9.4	9.6
log F _[O II] > -17.0	9.6	9.6	9.8
log F _[O II] > -16.5	9.7	9.5	9.5
log F _[O II] > -16.0	9.5	9.3	9.7

* See Fig. 13 for the presentation of stellar mass distributions for threshold fluxes of log F_{H_α} > -16.0 and log F_[O II] > -16.5.

mean values of $A_V = 1.2$ and emission line galaxies have larger extinctions in this figure. However the distribution of galaxies selected by [O II] at the lowest redshift range of $0.5 < z < 1.0$ shows a significant number of galaxies with $A_V \sim 0$ compared with other redshift ranges. It is uncertain whether this is real or caused by systematic uncertainties of photo- z calculation.

We also calculate the histogram of FWHM sizes of the SXDF galaxies in the three redshift ranges, as shown in Figure 15. One can compare these sizes with the fiber aperture or slit width in a planned survey to estimate the loss of emission line light due to the extended size of galaxies. The FWHM size was measured in the B band, because the galaxy profile in the shortest wavelength is expected to be close to that in emission lines. Seeing (~ 0.8 arcsec FWHM) has not been subtracted, meaning the values correspond to the actual image size under realistic observing conditions. In Figure 15, every distribution of FWHM size has a lower cut-off at approximately 0.75 arcsec and gradually decays with increasing size. The lower cut-off is due to the original image quality of the optical images in SXDF. For reference, the fiber diameter of FMOS is 1''.2 diameter, and the planned fiber diameter of WFMOS is also about 1''. These results indicate that a significant fraction of emission line flux could be lost out of the fibers in large size galaxies, and this effect must be taken into account in BAO survey planning.

5.4. Linear Bias

The bias of clustering is important to estimate the detectability of BAO signatures. We therefore calculate linear bias of clustering by using the baryon mass estimate of galaxies in SXDF. The baryon mass is estimated from the photometric redshift calculations, including stellar mass and gas mass that is not yet converted into stars. (In the case of the SED template of constant SFR, we suppose that gas mass is equal to the stellar mass estimated from the phot- z calculations.) The estimated mean gas mass is consistent with that of UV-selected galaxies at $z \sim 2$ obtained by Erb et al. (2006). We then make a rough estimate of dark matter halo mass, assuming the cosmic baryon-to-DM ratio, $\Omega_b/\Omega_{\text{DM}}$:

$$M_{\text{DM}} = \frac{\Omega_{\text{DM}}}{\Omega_b} (M_* + M_{\text{gas}}),$$

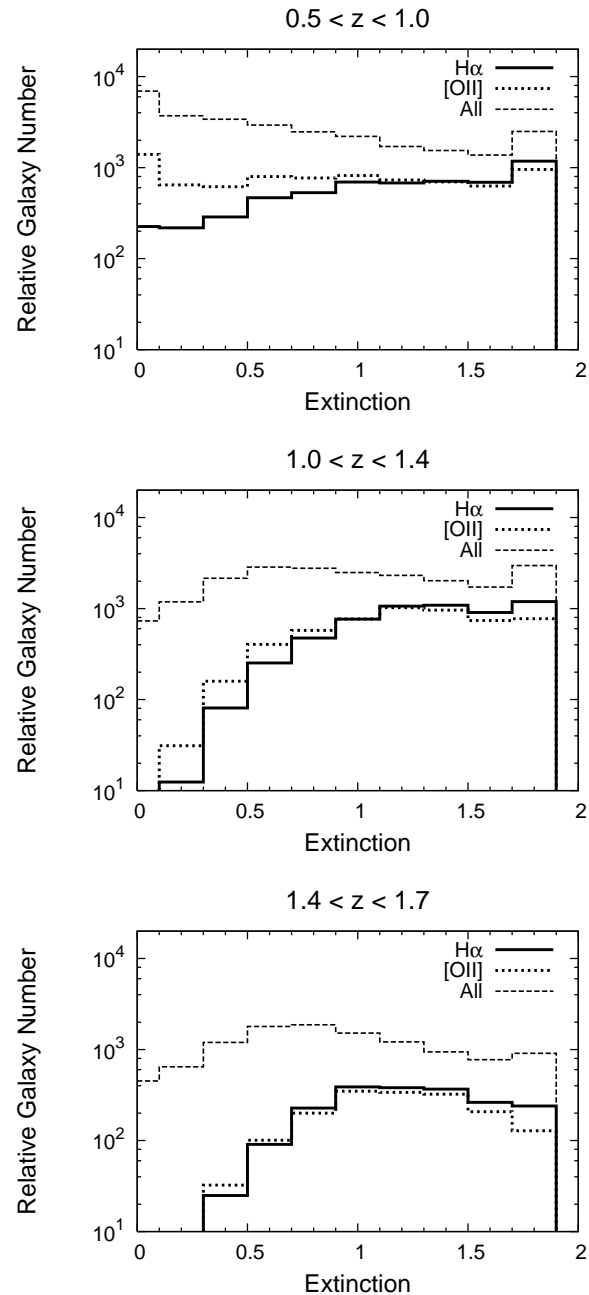


Fig. 14. The same as Fig. 13, but for the extinction (A_V) distributions of H_α and [O II] emission galaxies.

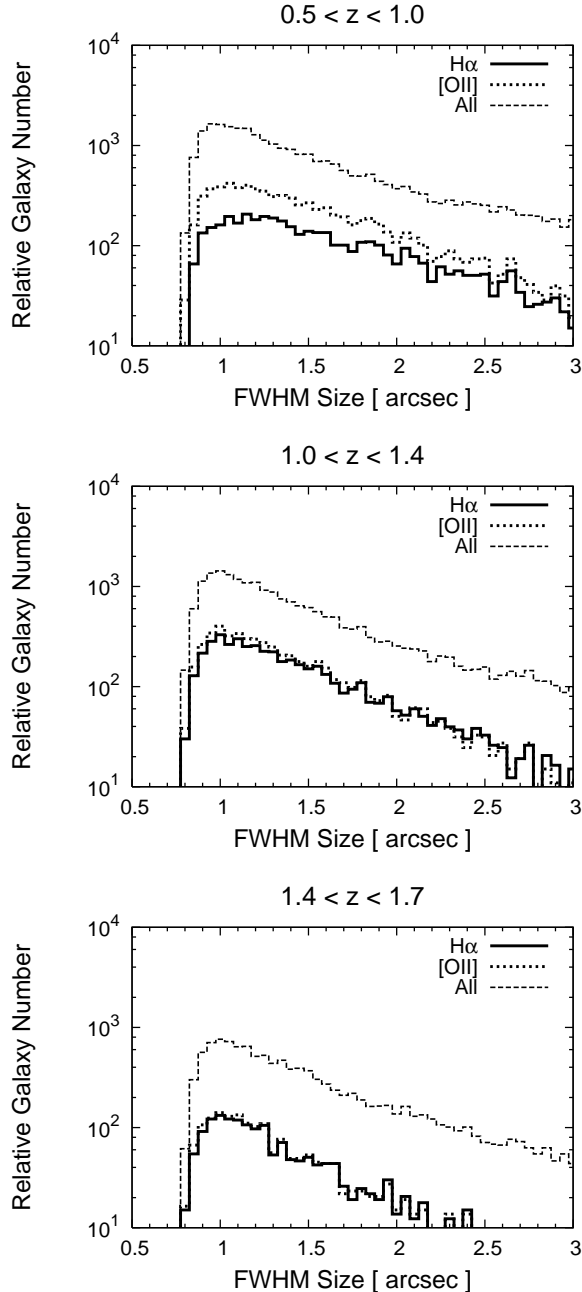


Fig. 15. The same as Fig. 13, but for the B -band FWHM size distributions of H α and [O II] emission galaxies. The seeing is not deconvolved in these sizes.

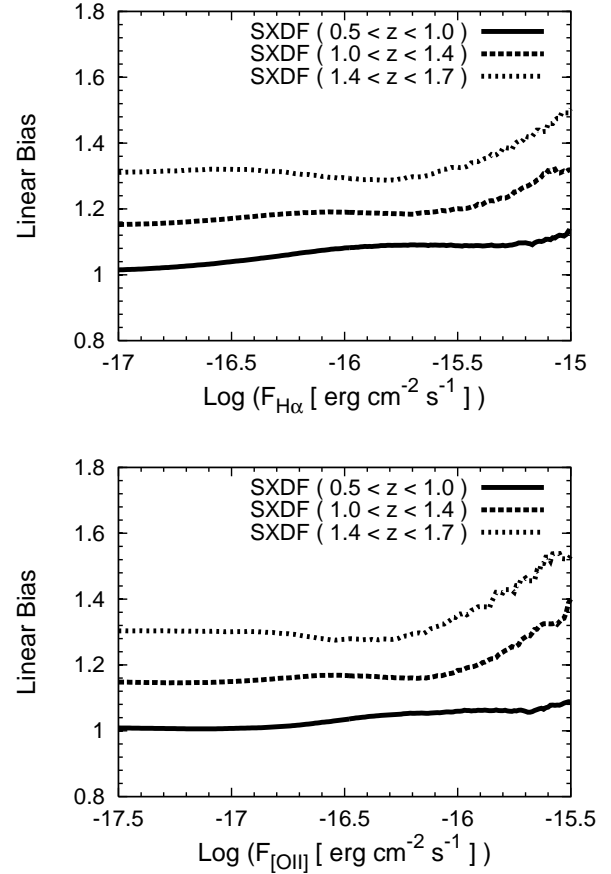


Fig. 16. The top panel shows the linear bias estimated for the SXDF galaxies that are brighter than a given H α flux, for the three redshift intervals as indicated in the panel. The bottom panel is the same as the top, but for the [O II] line.

where $\Omega_{\text{DM}} = \Omega_m - \Omega_b$, and Ω_m and Ω_b are the density parameters for matter and baryons, respectively. We then calculate the logarithmic mean of dark halo mass for a given threshold line flux in a given redshift interval, and then calculate linear bias from the estimated mass using the bias model of dark matter haloes of Cooray & Sheth (2002). The biases estimated in this way are shown in Figure 16 for the SXDF galaxies as functions of the threshold H α and [O II] fluxes. The estimated linear bias is typically $b \sim 1-1.5$. Since the stellar mass of galaxies does not change with the threshold flux or redshift, the linear bias does not depend strongly on the threshold flux, but it becomes larger at higher redshifts.

We estimated the linear bias assuming that the DM-to-baryon mass ratio of galaxies is the same as the cosmic value, but it may not be the case, and it is likely an underestimation because of the following reasons. First, the gas mass estimated by the star formation history of photo-z templates (exponential SFR evolution) is highly uncertain, and gas mass can be much larger than stellar mass in young, line-emitting starburst galaxies (Erb et al. 2006). Second, we have implicitly assumed that all the baryons are either in stars or in cold gas participating in star-formation. However, a significant amount of diffuse

hot gas could also lie in dark halos. It has been found empirically that the ratio of dark halo and stellar mass is approximately $2\text{--}20\Omega_{\text{DM}}/\Omega_b$ for different luminosities of galaxies at $z \sim 2$ (e.g., Hayashi et al. 2007). Therefore we also calculate the biases with a 3 and 10 times larger DM mass than the above estimates, but the linear biases are only modestly increased by 10% and 30%, respectively.

We can compare the bias estimates with those by clustering analysis in the literature at $z \simeq 1.0\text{--}2.0$, by converting correlation length into bias of line-emission galaxies. Blake et al. (2009) obtained $b \sim 1.6$ for [O II] emitters at $z = 0.5\text{--}1.0$ from the real space correlation function of the WiggleZ project data (Glazebrook et al. 2007; Blake et al. 2009), with a threshold [O II] flux of 1 hour integration on the 3.9m Anglo-Australian Telescope ($\sim 10^{-16}\text{erg cm}^{-2}\text{s}^{-1}$). This bias is larger than our estimate, and this can not be explained by increasing the DM-to-baryon mass ratio of galaxies. However, this is likely to be due to the strong additional r -band selection criteria of the WiggleZ survey ($20 < r < 22.5$). We found that, when we add $20 < r < 22.5$, our bias estimate is increased by 20% as well. Therefore, our bias estimate is in rough agreement with the WiggleZ clustering data when the increase of our bias prediction by larger $\Omega_{\text{DM}}/\Omega_b$ values is taken into account. Geach et al. (2008) obtained $b = 2.0$ for H α emitters at $z \sim 2.2$ by angular correlation function, with a threshold H α flux of $\sim 10^{-16}\text{erg s}^{-1}\text{cm}^{-2}$. This is out of the redshift range that we investigated, but it seems also roughly consistent with our estimate considering the increasing trend of bias with redshift.

5.5. Clustering Property

Next we examine the field-to-field variation of the observed number of emission-line galaxies in SXDF, and compare it with those expected from the linear bias estimated above and the CDM structure formation theory. A detailed study on the clustering properties by using angular correlation function will be reported elsewhere. We divided the region in SXDF used in this work (the region having both optical and NIR data) into four sub-regions (SXDF 1–4) with roughly the same area of $\sim 0.18\text{ deg}^2$ (see Figure 17 and Table 3).

We then estimate the standard deviation $\sigma_{\text{gal,obs}}$ of the galaxy density fluctuation $\delta_{\text{gal}} = \delta\rho_{\text{gal}}/\bar{\rho}_{\text{gal}}$ on the volume scale of the sub-fields as follows. When the surface galaxy number density n_i in the i -th sub-field obeys a distribution with the mean value \bar{n} , the unbiased estimate for the standard deviation σ_n of the distribution from the observed number densities is given by:

$$\sigma_n^2 = \frac{1}{N-1} \sum_{i=1}^N (n_i - \bar{n}_{\text{obs}})^2, \quad (1)$$

where $\bar{n}_{\text{obs}} = \sum n_i/N$ is the observational estimate of the mean value. Then, $\sigma_{\text{gal,obs}}$ is simply estimated by $\sigma_n/\bar{n}_{\text{obs}}$. The observational error in the $\sigma_{\text{gal,obs}}$ estimate can be calculated by approximating that $\sum(n_i - \bar{n}_{\text{obs}})^2/\sigma_n^2$ obeys to χ^2 distribution with $N-1$ degrees of freedom. The value of $\sigma_{\text{gal,obs}}$ and its error are thus esti-

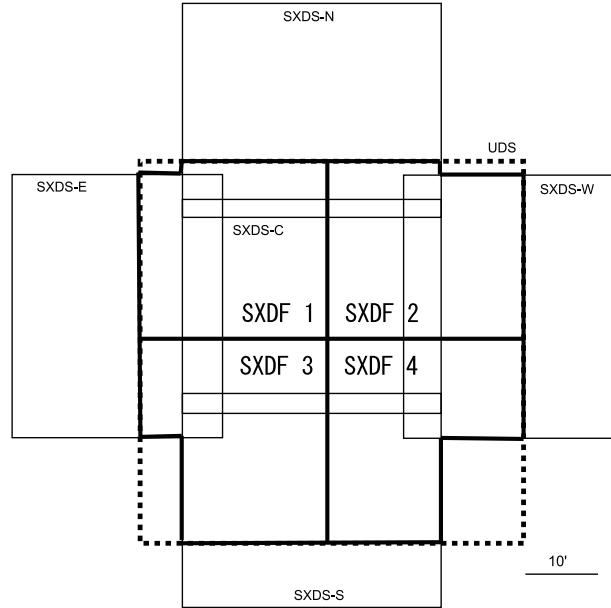


Fig. 17. Overview of SXDF. The regions indicated by thin solid lines are the five fields of view of Subaru/Suprime-Cam (SXDS-C, N, S, W, and E). The region shown by dashed lines is the area where NIR data by UKIRT/WFCAM is available. All of the field is covered by mid-infrared observations by Spitzer/IRAC. We used the overlapping region of the optical and NIR data, and the thick solid lines show the four sub-fields defined in this work.

mated for galaxies brighter than $10^{-16}\text{erg cm}^{-2}\text{s}^{-1}$ (H α) and $10^{-16.5}\text{erg cm}^{-2}\text{s}^{-1}$ ([O II]), which are given in Table 3 in the three redshift ranges.

To compare with these results, we calculate the theoretically expected standard deviations, $b\sigma_{\text{CDM}}$, where σ_{CDM} is the standard deviation of dark matter fluctuation and b is the linear bias of line emitting galaxies. The value of σ_{CDM} is calculated assuming a spherical top-hat window function with radius R , and R is assumed to be $R = (3V/4\pi)^{1/3}$, where V is the averaged volume of the four sub-fields of SXDF. The results are given in Table 3, to be compared with $\sigma_{\text{gal,obs}}$. The values of $b\sigma_{\text{CDM}}$ are in agreement with $\sigma_{\text{gal,obs}}$ in $1.0 < z < 1.4$ and $1.4 < z < 1.7$, but in disagreement in $0.5 < z < 1.0$. The origin of the discrepancy only in $0.5 < z < 1.0$ is not clear, but the estimate of $\sigma_{\text{gal,obs}}$ is based only on four subfields. We find that the chance probability of getting this level of deviation is about 4% and 20% for H α and [O II] line cases, respectively, and hence the possibility of a statistical fluke cannot be excluded.

6. Example of Color Selection

Actual selection procedures in a particular BAO survey will depend on various conditions that are unique to the survey, such as available band filters of input imaging surveys. Therefore it is difficult to derive generally useful results, but here we test some simple two-color selection methods to select emission line galaxies brighter

Table 3. Field-to-field variation of galaxy number

Field	Area [deg 2]	Galaxy Number in Each Field					
		log $F_{\text{H}\alpha}^*$ ≥ -16.0			log $F_{\text{[O II]}}^*$ ≥ -16.5		
		$z=0.5\text{--}1.0$	$z=1.0\text{--}1.4$	$z=1.4\text{--}1.7$	$z=0.5\text{--}1.0$	$z=1.0\text{--}1.4$	$z=1.4\text{--}1.7$
SXDF 1	0.179	1130	1361	386	1523	1238	331
SXDF 2	0.199	1235	1311	371	1768	1241	322
SXDF 3	0.176	1119	1044	419	1610	1005	358
SXDF 4	0.178	1134	907	394	1691	850	328
$\sigma_{\text{gal,obs}}$ \dagger		0.012	0.168	0.099	0.047	0.153	0.093
$\Delta\sigma_{\text{gal,obs}}$ \ddagger			± 0.009	± 0.137	± 0.081	± 0.038	± 0.124
$b\sigma_{\text{CDM}}$ \S			0.125	0.105	0.104	0.120	0.103
* In units of line flux [erg cm $^{-2}$ s $^{-1}$].							

\dagger The standard deviation of galaxy density fluctuation, $\delta\rho_{\text{gal}}/\bar{\rho}_{\text{gal}}$ estimated from the observed galaxy numbers in sub-fields.

\ddagger The observational error of $\sigma_{\text{gal,obs}}$.

\S The expected density fluctuations predicted from the CDM theory and the bias estimates, which should be compared with $\sigma_{\text{gal,obs}}$.@

than $F_{\text{H}\alpha} \geq 10^{-16}$ erg cm $^{-2}$ s $^{-1}$: one is using only optical photometries ($Bi'z'$), and the other is including the NIR K band ($Bz'K$). We do not show in detail the results for [O II], but we have confirmed that the results are similar when one considers the corresponding [O II] line flux of $10^{-16.5}$ erg cm $^{-2}$ s $^{-1}$.

Before we examine the two-color diagrams, we should select relatively bright galaxies as potential targets for BAO surveys, using photometric information. From the magnitude distribution of emission-line galaxies (Figure 11), we set the magnitude threshold as $B < 24$. We then show the color-color diagrams of all the SXDF galaxies with $B < 24$ for the two cases, in Figure 18 and Figure 19. Galaxies that are brighter than $F_{\text{H}\alpha} = 10^{-16}$ erg cm $^{-2}$ s $^{-1}$ are shown by colored dots, for the three different redshift intervals. From these results, we define the color selection criteria to efficiently select the emission-line galaxies, as shown by the box in the same colors for the three redshift intervals. These criteria were chosen not only by the number of target emission line galaxies, but also by the expected success rate examining the contamination of non-emission line galaxies (black dots). These criteria can also be applied for [O II] emitters brighter than $10^{-16.5}$ erg cm $^{-2}$ s $^{-1}$ because the distributions on the two-color planes are similar to those in the H α cases.

Figures 20 and 21 show the number of emission-line galaxies brighter than three threshold H α line fluxes of $10^{-15.5}$, 10^{-16} , and $10^{-16.5}$ erg cm $^{-2}$ s $^{-1}$, as a function of the threshold B magnitude when we select galaxies by these color criteria. It can be seen that for the two low redshift bins sufficient galaxies ($nP \gtrsim 1$) are obtained at a depth of $B = 24$ with a 10^{-16} erg cm $^{-2}$ s $^{-1}$ threshold. For the highest redshift bin we need to go deeper ($B = 25$) to attain sufficient galaxies.

The success rate of the selection, i.e., the fraction of galaxies having larger emission line flux than the threshold and in the correct redshift range is also shown in these figure, compared with the total number of all galaxies satisfying the B magnitude threshold and color selection criteria. These results indicate that typically a success rate of about 40% in the two low redshift bins can be achieved

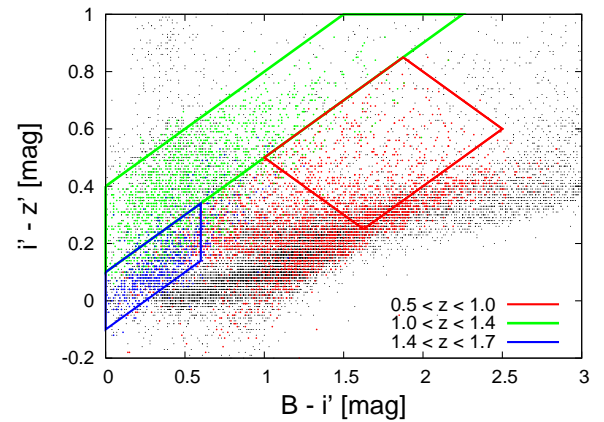


Fig. 18. The $Bi'z'$ plot for SXDF galaxies with $B < 24$. Galaxies with H α flux brighter than 10^{-16} erg cm $^{-2}$ s $^{-1}$ in the three redshift ranges are indicated by red, green, and blue dots, while the other galaxies in black dots. The color selection criteria used for the three redshift ranges are indicated by the corresponding colors.

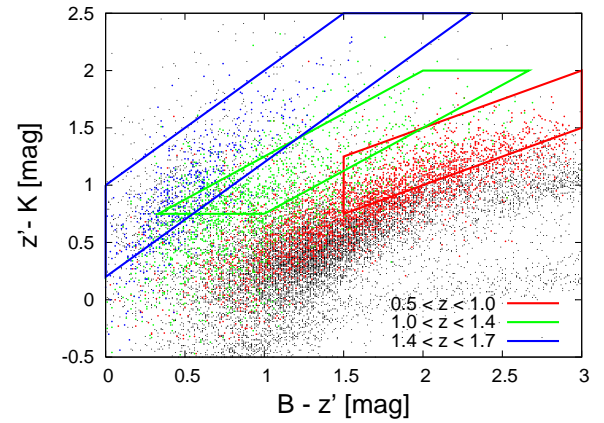


Fig. 19. The same as Figure 18, but for $Bz'K$ diagram.

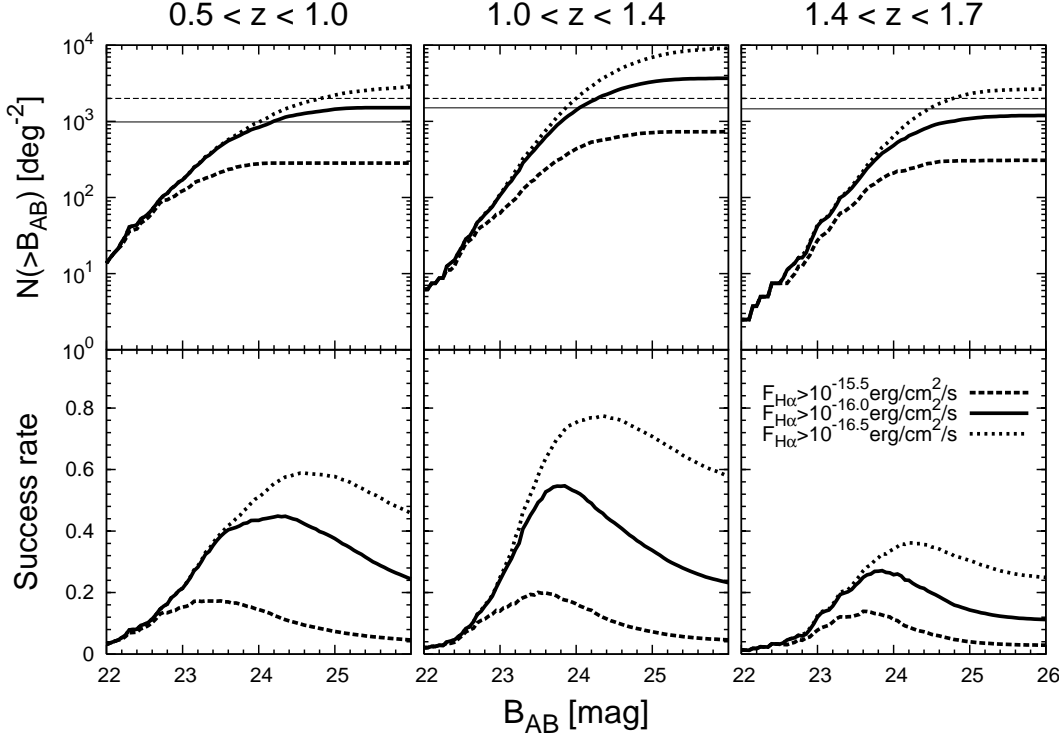


Fig. 20. The counts and probability of successful selection in the three redshift intervals by the $Bi'z'$ selection method, for galaxies brighter than a given threshold B magnitude (abscissa). The galaxy sample is SXDF. The horizontal lines (solid and dashed) in the top panels indicate the surface number density corresponding to $n_P = 1$ at each redshift interval and the FMOS fiber density, respectively. The dashed, solid, and dotted lines are for the three threshold $H\alpha$ fluxes of $10^{-15.5}$, $10^{-16.0}$, and $10^{-16.5}\text{erg cm}^{-2}\text{s}^{-1}$, respectively.

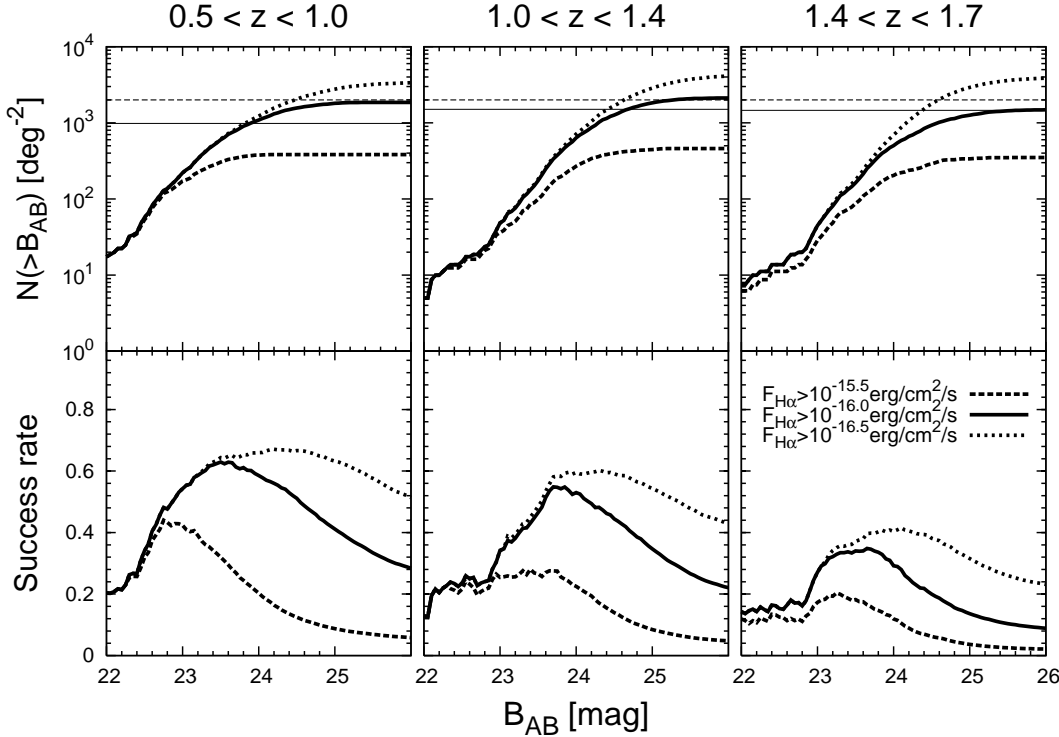


Fig. 21. The same as Fig. 20, but for the $Bz'K$ selection.

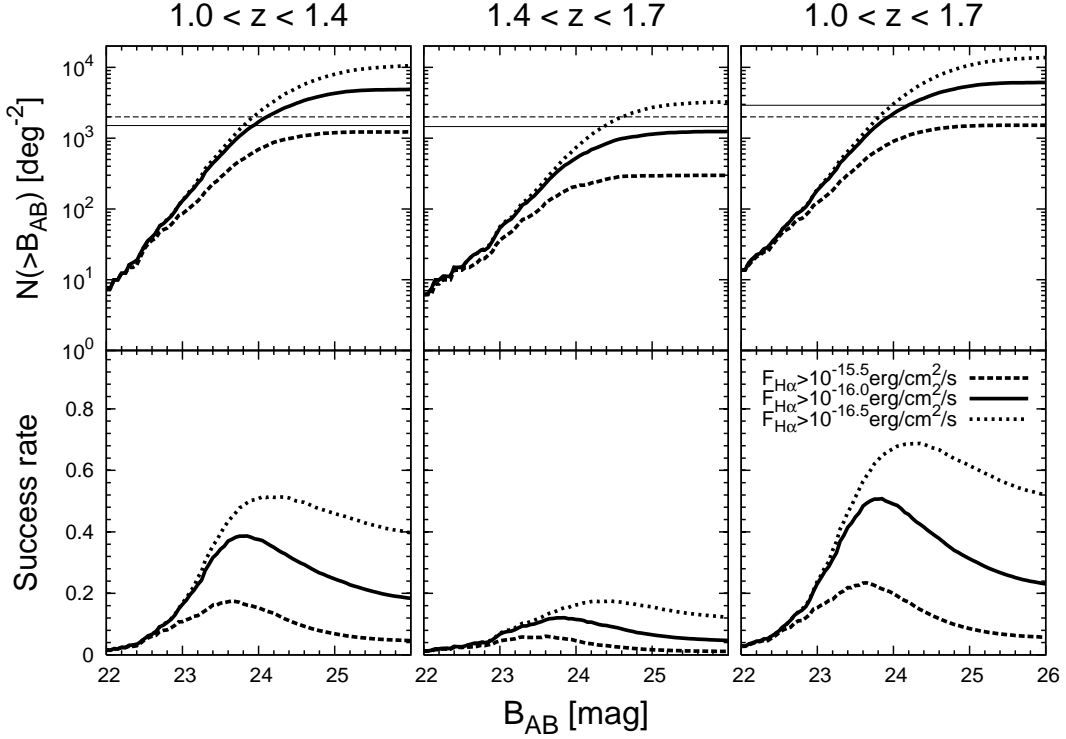


Fig. 22. The same as Fig. 20, but for the $Bi'z'$ selection on the $1.0 < z < 1.7$ joint condition. The left, middle, and right panels show the counts and probability of the successful selection for galaxies in the redshift intervals of $1.0 < z < 1.4$, $1.4 < z < 1.7$, and in the joint redshift interval of $1.0 < z < 1.7$.

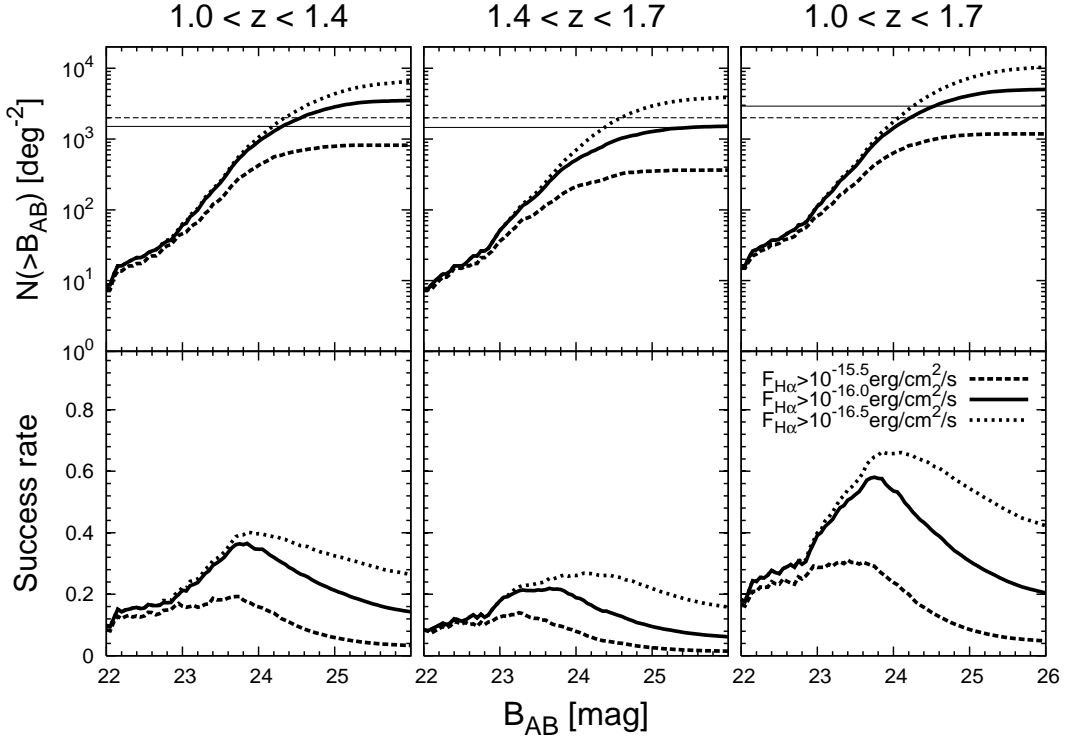


Fig. 23. The same as Fig. 22, but for the $Bz'K$ selection on the $1.0 < z < 1.7$ joint condition.

by this simple color selection for the threshold line flux of $F_{\text{H}\alpha} = 10^{-16} \text{ erg cm}^{-2} \text{s}^{-1}$. For the case for [O II], we also find that typically a success rate of about 40% in the two low redshift bins can be achieved for the threshold line flux of $F_{[\text{O II}]} = 10^{-16.5} \text{ erg cm}^{-2} \text{s}^{-1}$.

Finally we consider the two-color selection for high redshift galaxies at $z = 1\text{--}1.7$ using $Bi'z'$ and $Bz'K$ photometries. This may be effective if we do not discriminate galaxies beyond or below $z = 1.4$ and are simply interested in selecting galaxies at $z > 1$. We define the selection criteria for $Bi'z'$ and $Bz'K$ as shown by the two high redshift boxes in Figure 18 and 19, respectively. From Figure 22 and 23, we can select a sufficient number of galaxies at $1.0 < z < 1.7$ by a survey deeper than $B = 24$ with a success rate of 50–60%. If the survey depth is deeper than $B = 25$, we can select a sufficient number of galaxies both in the two redshift intervals of $1.0 < z < 1.4$ and $1.4 < z < 1.7$.

We find that both $Bi'z'$ and $Bz'K$ selection deliver comparable performance for selection in terms of magnitude depth required and success rate. The choice would then come down to the ease of obtaining the observational datasets.

Possible improvements would be to try three-color selection boxes, or multi-parameter methods in an N -dimensional photometric space. These improvements are beyond the scope of this paper but we will explore such possibilities in future work.

7. Summary

We made an estimate of $\text{H}\alpha$ and [O II] emission line luminosities of SDF and SXDF galaxies in a total field area of 0.846 deg^2 by a photometric redshift based approach, for the purpose of studying photometric selection procedures of high redshift emission line galaxies useful for future spectroscopic BAO surveys. Our line luminosity estimates were tested and calibrated by using the SDSS galaxies with spectroscopic line luminosity measurements at low redshifts. The line luminosity functions of $\text{H}\alpha$ and [O II] were thus derived in three redshift intervals in $z = 0.5\text{--}1.7$, and they are in reasonable agreement with the previous studies based on spectroscopic or narrow-band filter observations.

We examined the number density and properties of emission line galaxies that can be used for future BAO surveys, taking FMOS and WFMOS instruments for the Subaru Telescope as representative examples. We have confirmed that there are sufficient number of emission line galaxies to perform BAO surveys in the redshift ranges $0.5 < z < 1$ and $1 < z < 1.4$ which are bright enough to be detected by 8–10 m class telescopes with exposures shorter than one hour. We showed cumulative distributions of magnitudes in popular band filters for emission line galaxies with line flux brighter than given thresholds in a range of redshift intervals, and these can be used to estimate the required depth of an imaging survey from which spectroscopic targets are selected.

We also estimated the stellar mass distributions, extinction distributions, FWHM size distributions, and linear

biases of line emitting galaxies. The linear biases were inferred from the stellar mass and redshift estimates, combined with the standard theory of structure formation. The inferred biases are consistent with the field-to-field variation of galaxy numbers in four subfields in SXDF, and also with the estimates based on clustering analysis for similar galaxies in previous studies.

Finally, we showed some examples of color selection of target galaxies for spectroscopic BAO surveys, based on simple color-color selections ($Bi'z'$ and $Bz'K$). It is found that target galaxies for BAO surveys can be selected with a reasonable accuracy and success rate. We find that with this selection for $z < 1.4$ we need to reach a typical depth of $B = 24$ (with other filters being required for color-selection) and for $1.4 < z < 1.7$ we need to reach $B = 25$. We find the $Bi'z'$ and $Bz'K$ selection methods give comparable efficiency. In general we find that it is not possible to efficiently select galaxies in the high-redshift $1.4 < z < 1.7$ using only two-colour selection.

These results give guidance for the planning of future BAO surveys and demonstrate that 8-m telescopes with spectroscopic fields of view of order one degree (instruments such as FMOS and WFMOS) would be effective machines for carrying out such large cosmological surveys.

The data of photometric magnitudes, redshifts, and line luminosities used in this work are available on request to the authors.

We would like to thank K. Harikae for useful discussions and E. Wisnioski for providing us with the observational results of WiggleZ survey. This work was supported by the Global COE Program "The Next Generation of Physics, Spun from Universality and Emergence" and Grant-in-Aids for Scientific Research (Nos. 19740099 and 20040005) from the Ministry of Education, Culture, Sports, Science and Technology (MEXT) of Japan. This work was also supported by the Japan Society for Promotion of Science (JSPS) Core-to-Core Program 'International Research Network for Dark Energy'. Karl Glazebrook acknowledges support for this work from Australian Research Council (ARC) Discovery Projects DP0774469 and DP0772084.

References

- Adelman-McCarthy, J. K., et al. 2006, ApJS, 162, 38
- Akiyama, M., et al. 2009, in preparation
- Baldry, I. K., & Glazebrook, K. 2003, ApJ, 593, 258
- Bassett B. A., Nichol R. C., & Eisenstein D. J. 2005, preprint (astroph/0510272)
- Bertin E. & Arnouts S. 1996, A&AS, 117, 393
- Blake, C. & Glazebrook, K. 2003, ApJ, 594, 665
- Blake, C., et al. 2009, MNRAS in press (astroph/09012587)
- Bolzonella, M., Miralles, J. M., & Pello, R. 2000, A&A, 363, 476
- Brinchmann, J., et al. 2004, MNRAS, 351, 1151
- Bruzual, G. & Charlot, S. 2003, MNRAS, 344, 1000
- Calzetti, D., et al. 2000, ApJ, 533, 682
- Cole, S., et al. 2005, MNRAS, 362, 505
- Cooray, A. R. & Sheth, R. 2002, Phys. Rep., 372

- Copeland, E.J., Sami, M., Tsujikawa, S., 2006, *Int. J. Mod. Phys. D* 15, 1753
- Eisenstein, D. J. & Hu, W. 1998, *ApJ*, 496, 605
- Eisenstein D., White M., 2004, *Physical Rev. D*, 70, 103523
- Eisenstein, D. J., et al. 2005, *ApJ*, 633, 560
- Eisenstein, D. J., et al. 2006, *ApJS*, 167, 40
- Erb, D. K., et al. 2006, *ApJ*, 646, 107
- Eto, S., et al. 2004, *Proc. SPIE*, 5492, 1314
- Furusawa, H., et al. 2008, *ApJS*, 176, 1
- Geach, J., E., et al. 2008, *MNRAS*, 388, 1473
- Glazebrook K., Blake C.A. & Dalton G.B. 2004a, in *Proc. of the FMOS Science Workshop 2004*, ed. Maihara & Ohta, Kyoto University Press, p. 134-140
- Glazebrook, K., et al. 2004b, *Nature*, 430, 181
- Glazebrook, K. & Blake, C. 2005, *ApJ*, 631, 1
- Glazebrook, K., et al. 2007, *ASPC*, 379, 72
- Hayashi, M., et al. 2007, *ApJ*, 660, 72
- Hippelein, H., et al. 2003, *A&A*, 402, 65
- Hogg, W. D., et al. 1998, *ApJ*, 504, 622
- Hopkins, A. M., Connolly, A. J. & Szalay, A. S. 2000, *ApJ*, 120, 2843
- Hopkins, A. M., et al. 2003, *ApJ*, 599, 971
- Ilbert, O., et al. 2006, *A&A*, 457, 841
- Iwamuro, F., et al. 2008, *Proc. SPIE*, 7014, 26
- Kashikawa, N., et al. 2004, *PASJ*, 56, 1011
- Kennicutt, R. C. 1998, *ARA&A*, 36, 189
- Kewley, L. J., Geller, M. J. & Jansen, R. A. 2004, *ApJ*, 127, 2002
- Komatsu, E., et al. 2008, submitted to *ApJS*(astro-ph/08030547)
- Lonsdale, C., et al. 2004, *ApJS*, 154, 54
- Ly, C., et al. 2007, *ApJ*, 657, 738
- Motohara, K., et al. 2009, in preparation
- Moustakas, J., Kennicutt, R. C., & Tremonti, C. A. 2006, *ApJ*, 642, 775
- Nagashima, M. & Yoshii, Y. 2004, *ApJ*, 610, 23
- Okumura, T., et al. 2008, *ApJ*, 676, 889
- Parkinson, D., et al. 2007, *ApJ*, 377, 185
- Percival, W. J., et al. 2007, *ApJ*, 657, 645
- Perlmutter, S., et al. 1999, *ApJ*, 517, 565
- Riess, A. G., et al. 1998, *AJ*, 116, 1009
- Salpeter, E. E. 1955, *ApJ*, 121, 161
- Schlegel, D. J., Finkbeiner, D. P., & Davis, M. 1998, *ApJ*, 500, 525
- Seo, H. J. & Eisenstein, D. J. 2003, *ApJ*, 598, 720
- Spergel, D. N., et al. 2007, *ApJS*, 170, 377
- Takahashi, M. I., et al. 2007, *ApJS*, 172, 456
- Tegmark, M., et al. 2006, *Phys. Rev. D*, 74, 123507
- Teplitz, I. H., et al. 2003, *ApJ*, 589, 704
- Tresse, L., et al. 2002, *MNRAS*, 337, 369
- Warren, S., et al. 2007, *MNRAS*, 375, 213
- Yan, L., et al. 1999, *ApJ*, 519, L47
- Zhu, G., et al. 2008, submitted to *ApJ*(astro-ph/08113035)